DESIGN, FABRICATION, AND VALIDATION OF A PORTABLE PERTURBATION TREADMILL FOR BALANCE RECOVERY RESEARCH

by

Robert George Knutson

A thesis submitted in partial fulfillment
of the requirements for the degree

of

Master of Science

in

Mechanical Engineering

MONTANA STATE UNIVERSITY
Bozeman, Montana

December 2022

DEDICATION

Several people need to be thanked for helping make this project a success. First, my advisor, Corey Pew, for a master class in technical writing. Next, my committee, David Graham, and Craig Shankwitz, for listening to my ideas and providing guidance when needed. Finally, my copy editor, brainstorming buddy, and lovely wife, Elisabeth Knutson, for putting up with my engineering jargon and impromptu physics lectures all these years.

I would like to dedicate this work to all the aspiring engineers, the tinkers, the people who just want to know how the world works. Never stop learning, never stop questing, always try to make something new.

ACKNOWLEDGEMENTS

Research reported in this publication was supported by the National Institute of General Medical Sciences of the National Institutes of Health under Award Number P20GM103474. The content is solely the responsibility of the authors and does not necessarily represent the official views of the National Institutes of Health.

TABLE OF CONTENTS

1. INTRODUCTION 1

General Overview 1
Background and Motivation 1
General Balance Training & Perturbation Balance Training 2
Perturbation Device Requirements 3
Statement of the Problem 6
Purpose 6

2. METHODS 7

Functional Requirements 7
Portability 8
Perturbation Response Testing 9

3. RESULTS 10

Functional Requirements 10
System Overview 10
Motor Control & System Cost 12
Verification of Performance 13
Portability 14
Perturbation Response Testing 15

4. DISCUSSION 16

Functional Requirements 16
Portability 18
Perturbation Response Testing 18

5. CONCLUSION 19

6. APPENDICES 20

APPENDIX A: INDUSTRY DESIGN GUIDELINES 21
What is a Treadmill Belt? 22
Conveyor Belt Tracking 22
Belt Tension 24
Shortcomings of Euler- Eytelwein Formula 25
Belt Creep 26
APPENDIX B: DETAILED MOTOR & PULLEY CALCULATIONS 27

TABLE OF CONTENTS CONTINUED

Introduction 28
Analysis Setup 28
User Information and Design Values 29
Drum Selection 30
Drive Belt and Gearing Selection 31
Motor Selection 32
Kinetic Energy of Objects in Rotational Motion. 33
Kinetic Energy of Objects in Translational Motion. 35
Torque and Total Kinetic Energy. 36
Selected Motor Features 37
Motor Control Methods 37
APPENDIX C: DETAILED BELT TENSION CALCULATIONS 39
Dimensional Considerations & Analysis Setup 40
Calculating Minimum Belt Width 40
Calculating Required Belt Tension 42
Catenary Load 43
Determining Maximum Belt Elongation Under Load 45
Determining Total Initial Belt Preload 48
Notes On Preload and Tension Calculations. 49
APPENDIX D: DETAILED SHAFT DESIGN CALCULATIONS 50
Introduction 51
Loads 53
Shear and Moment Assumptions and Diagrams 53
Endurance Limit and Shaft Size 55
Notes on Shaft Sizing 57
APPENDIX E: DETAILED BEARING CALCULATIONS 58
Introduction 59
Assumptions 59
Calculations and Bearing Selection 59
Notes on Bearing Selection 61
APPENDIX F: DETAILED FRAME ANALYSIS 62
Introduction 63
Background 63
Assumptions 65
Calculations for Outer Members 65
Calculations for Inner Member 67
Adjusting Belt Tension 68
Belt Tracking 70
APPENDIX G: DETAILED HMI DESIGN 73
Introduction 74
Components 75

TABLE OF CONTENTS CONTINUED

Anticipated Workflow 76
Wiring Diagram 77
APPENDIX H: DETAILED SOFTWARE DESIGN 78
Introduction 79
Motor Controller 79
Creating Perturbation Profiles 81
Motor Monitor 83
Software Notes 84
APPENDIX I: DETAILED DEVICE VALIDATION 85
Human Analog Test 86
Results of Human Analog Testing 87
Human Testing 88
Results of Human Test 89
APPENDIX J: SUMMARY TABLES, DATASHEETS, & BUDGET 90
Overview 91
Drivetrain 91
Bearings 91
Frame 92
Material Properties 92
User 92
Data From Human Test 93
Belt Design Software Datasheet 94
Treadmill Belt Data Sheet 95
Motor Wiring Pin Out 96
Budget 97

7. REFERENCES CITED 100

LIST OF TABLES

Table Page

1. Summary of User Demographic Information. 30
2. Inputs to Timing Belt Selection Software. 31
3. Summary of Masses and Moments of Inertia. 33
4. Details of the Selected Motor. 37
5. Summary of Shaft Sizing Results. 56
6. Published Data for Selected Bearings. 60
7. Criteria and Unit Loads for Column Buckling. 64
8. Summary of Properties for T-Slot Sections. 65

LIST OF FIGURES

Figure Page

1. Types of Perturbation Devices. 3
2. Example of Perturbation Belt Velocity Profiles. 4
3. Trip Slip Diagram. 5
4. Images of Completed Treadmill. 10
5. Front of Treadmill Showing Electrical Components. 11
6. Shaft Component Diagram. 11
7. Final Configuration of the Controller Module. 12
8. Matlab GUI for Creating Custom Perturbation Profiles. 13
9. Manual Treadmill Transport. 14
10. Setup for Human Subject Test. 15
11. Belt Tracking. 23
12. Lateral Guide Example. 24
13. Free Body Diagram of Belt Tension. 25
14. Front of Treadmill Showing Motors, Pulleys, & Timing Belts 28
15. Body Movement Diagrams. 29
16. Variables for Load Inertia Calculations. 32
17. Catenary Cable and Free Body Diagram. 44
18. Diagram of Belt Tension in Reverse Operation. 46
19. Graph of Belt Elongation Under Load. 47
20. Shaft Component Diagram. 51

LIST OF FIGURES CONTINUED

Figure Page

21. Characteristics of Fatigue Strength for Steel and Aluminum. 52

22. Shear and Moment Diagrams. 54

23. Areas of Interest for Fatigue Life Calculations. 56

24. Cross Section of Shaft Showing Recessed Bearing. 61

25. Pictures of the Frame. 63

26. Layout of the Inner Member. 67

27. Inner Member Front Connection. 67

28. Center Section Reinforcements. 68

29. Belt Tension Adjustment Locations. 69

30. Additional Center Tension Adjustment. 70

31. Initial Belt Tracking Method. 71

32. Additional Belt Tracking Methods. 71

33. Guides for Lower Belts. 72

34. Final Configuration of the Controller Module. 74

35. Workflow of HMI Buttons. 76

36. Control Box Wiring Diagram. 77

37. Code Flowchart. 80

38. Examples of Perturbation Profiles. 81

39. Graph of PWM Signal Sent to Motor. 82

40. Graphical User Interfaces Used to Display Motor Data. 83

LIST OF FIGURES CONTINUED

Figure Page

41. Linear Approximation of Trigonometric Function. 84

42. Human Analog Test.. 87

43. Setup for the Human Test.. 88

44. Motor Diagnostic Data Collected During Human Testing....................................... 89

ABSTRACT

Trips and falls are a major concern for older adults. The resulting injury and loss of mobility can have a significant impact on quality of life. An emerging field of study, known as Perturbation Training, has been shown to reduce injury rates associated with trips and falls in older adults. In a typical training session, the user stands or walks on a treadmill and is subject to sudden, unexpected accelerations, simulating a trip or slip, in a safe environment. This training aims to improve the user's ability to maintain and recover balance in situations that can often lead to falls.

Treadmills traditionally used for Perturbation Training are large instrumented devices that are rigidly bolted to the floor. This presents a problem for older adults with limited mobility or those who live far away from Perturbation Training facilities. A portable treadmill would be able to serve a larger portion of the at-risk population then current methods have allowed.

We developed a portable, low-cost perturbation treadmill capable of high-intensity training. The system can perform trip and slip perturbations from a stationary or walking state. It features a tandem belt configuration, a small gap between belts, and individual belt control. The belt speed is digitally controlled, dictated by a custom human-machine-interface and software suite, which allows operators with no programming experience to control the device. When connected to a 240-volt power supply, the maximum belt speed is approximately 3.6 m/s. The treadmill was designed to accommodate a user of up to 118 kg and provide a maximum acceleration of 12 m/s^2 under full load. The treadmill weighs approximately 180 kg and can be moved like a wheelbarrow, with handles in the back and wheels in the front. The design has been validated and was used in multiple locations in a clinical trial.

INTRODUCTION

General Overview

Older adults fall when they lose balance and are unable to produce a suitable movement that enables them to reestablish their base of support. There are several ways to train balance in older adults, the most effective is Reactive Balance Training (RBT). One RBT method is called Perturbation Training which is implemented by rapidly accelerating a treadmill belt from stationary. This forces the participant to take a rapid step to regain balance. While this is highly effective, there is a limitation regarding access to suitable training facilities. Therefore, this paper details the design, fabrication, and validation of a portable perturbation treadmill intended to increase access to RBT by taking training to participants instead of participants traveling to a training location. First, a summarized version of the design procedure will be presented in sections 1-5, with a detailed analysis, including mathematical calculations, in section six, the Appendix. A summary of the data used in all calculations, including links to electronic files, is included in Appendix J.

Background and Motivation

Falls are a common and significant health threat among older adults [1]. Nearly one out of every three people over 65 years old will fall annually, and in half of these cases, the falls are recurrent [2]. For adults over 80, this rate increases to nearly 50% [3]. Approximately 30% of falls in adults over the age of 65 will be injurious [3]. The most severe non-fatal injuries include hip fractures (and their comorbidities) which are known to double the average mortality rate for up to 12 years, with the most significant risk in the first year [4]. Therefore, falls are a substantial factor influencing the reduction in quality of life of older adults and present a significant burden on the healthcare system.

General Balance Training & Perturbation Balance Training

Falls occur because of backwards, forwards, and sideways loss of balance, and while there are multiple causes of falls, few are modifiable. For example, the condition of sidewalks, weather conditions (snow and ice), or the use of graduated lenses in eyewear all contribute to fall occurrence but are not feasible to modify across the breadth of the population. However, physical function, such as coordinated muscle activity, strength, and power, is demonstrated to decline with age [5]. Most importantly, physical function is a readily modifiable factor which has given rise to multiple fall-prevention exercise interventions for older adults. Accordingly, fall prevention programs such as Stepping On, Stay Active and Independent for Life, and many other Exercise-Based Balance Training (EBT) programs have been introduced across the country. In a recent systematic review, *Sherrington et al.,* reported that EBT programs reduce falls by 23% on average and require a relatively high training dose. If training totals less than 50 hours or 3x/week or does not provide an adequate challenge to balance, the fall rate reduction is estimated to be 6-7% [6]. Perturbation-based Balance Training (PBT) is a newer method of fall prevention. Unlike conventional EBT programs, which target the ability to maintain balance and deal with known balance disruptions, PBT targets reactive balance control. By inducing unexpected perturbations (balance disruptions), PBT allows participants to practice and improve balance recovery in a manner that is both highly specific to recovery from a real-world fall and occurs in a safe and controlled environment. Thus far, PBT has been highly effective in terms of fall risk reduction [7-9]. For example, a recent meta-analysis reported that PBT resulted in a 50%

reduction in fall rate on average, at a substantially lower training dose than EBT [8]. For instance, *Pai* and *Bhatt* reported a ~50% reduction in prospective fall incidence after a single session of PBT [7]. Additionally, *Lurie et al.* demonstrated that older adults who were referred to physical therapy for high fall risk and received PBT were at a 57% lower risk of injurious falls than those assigned to EBT [9]. Therefore, Perturbation Based Training is an effective and efficient form of exercise-related balance training.

Perturbation Device Requirements

Traditional perturbation devices have fallen into two categories, instrumented treadmills and moveable platforms (Fig. 1). Instrumented treadmills accelerate the belts under the user to induce a slip or trip. The advantage of using this type of device is that perturbations can be triggered at any phase of the natural gait cycle due to its potential for continuous movement [10]. When multiple directions of travel are needed, a platform-based approach can be used, where the user stands on a stationary platform that can rotate or translate. For this type of system, the user is less likely to anticipate the direction of motion [11].

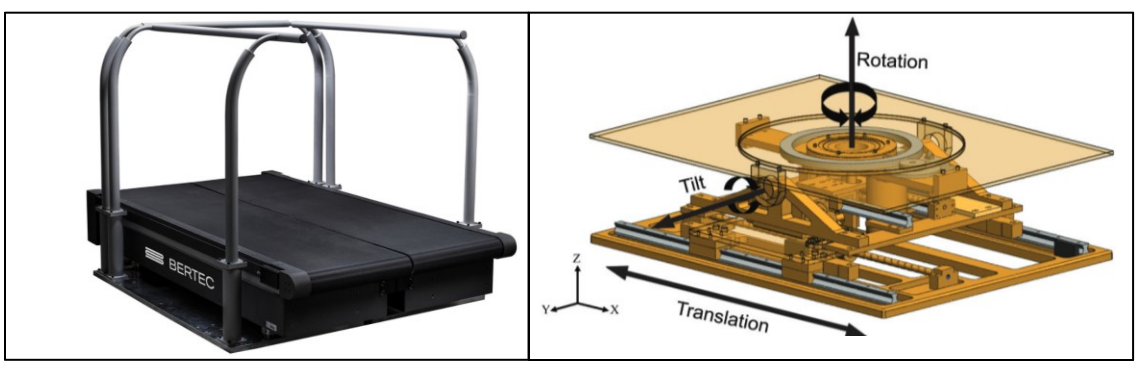

Figure 1. Types of Perturbation Devices.
Left. Instrumented treadmill [12]. Right. 5 DOF Moveable Platform [13].

There is an overall lack of PBT services in the commercial market. In the state of Montana, there is only one facility that advertises PBT. Considering that there are over 200,000 individuals 60 years or older in Montana [14], the market for PBT is currently underserved. Several factors could explain this, notably the initial cost and lack of portability of current devices. Standard exercise-grade treadmills are not suitable for PBT because training requires accelerations larger than standard treadmills can achieve [15]. While other PBT treadmills exist, their cost precludes them from overall market adaptation, limiting their use to dedicated research facilities. In addition, traditional PBT treadmills are not designed to be portable. This presents a problem for perturbation training because it requires the user to come to the treadmill, causing a barrier to implementing PBT for older adults in general, particularly older adults with limited mobility and those in rural or remote areas.

During a training session, the user will stand or walk on a moveable surface, such as a platform or treadmill, and will be exposed to sudden and unexpected accelerations. A typical training program consists of multiple sessions spread out over several weeks, and each session consists of multiple trials with varying intensities. The intensity of treadmill-based perturbations is varied by two factors, the acceleration of the belts and the duration of the perturbation (Fig. 2).

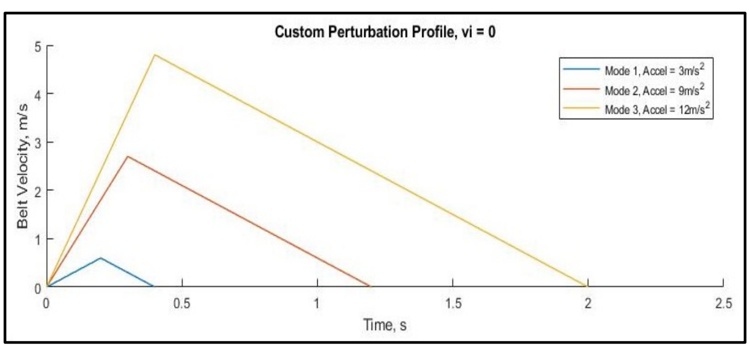

Figure 2. Example of Perturbation Belt Velocity Profiles. Different intensities can be achieved by varying the acceleration and total duration.

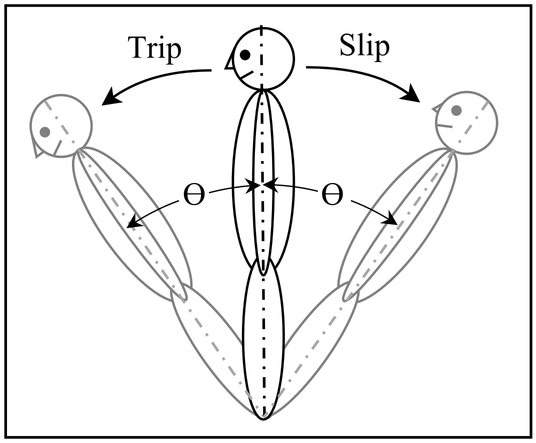

Figure 3. Trip Slip Diagram. Trips result in a forward loss of balance and slips result in a reward loss of balance. The trunk deflection angle, Θ, is measure relitive to an initial or resting state.

Treadmill-based perturbations are distinguished based on the real-world scenarios they intend to simulate. The two most common types are trip and slip perturbations (Fig. 3). Slips commonly occur at heel strike when the friction between the foot and the floor is less than the friction required for walking [16]. Typically this scenario results in a backward loss of balance [17]. Alternatively, trips commonly occur when an obstruction impedes the forward motion of the limb swing during gait, resulting in a forward loss of balance [18]. Both types of perturbations have been shown to elicit improved balance recovery and reduced fall rates in laboratory environments [19, 20]. The resultant motion can be quantified in terms of the maximum trunk flection angle relative to an initial or resting state [21], shown as Θ in Figure 3. Studies have shown that for the stimulus to improve balance recovery performance successfully, a minimum of approximately 25° of total trunk flection is required [21-23].

Statement of the Problem

Fall incidence is a large and growing problem that costs the healthcare system a substantial amount annually. This problem is projected to grow significantly with our generally aging population. Reducing the burden of falls requires strategies to improve the physical function and balance recovery performance of older adults. While general exercise balance training does work, its efficacy is limited. A newer balance training method called Perturbation Balance Training is demonstrated to be substantially more effective. However, its effectiveness has been limited because PBT requires large, expensive, and inaccessible training devices. This presents a clear need to develop a low-cost and accessible training solution.

Purpose

The purpose of this study/thesis was to design, build, and validate a low-cost and portable PBT treadmill capable of inducing high-intensity perturbations equivalent to those performed by commercial devices.

METHODS

The design of the PPT was guided by the need to create a functional, portable device capable of inducing postural responses similar to falls and slips.

Functional Requirements

A dual belt system was specified to allow independent perturbations to each lower limb. Each belt should be capable of supporting the full load of the user on a single lower limb. The PPT needed to accommodate a 118 kg (262 lb) user, encompassing 95% of people over 65 years old [24]. The system was designed to achieve high-intensity slip or trip perturbations with a maximum belt acceleration of 12 m/s^2 [25-27]. The three most critical components to select were the motors, shafts, and belts. The motors require digital speed control so the belt speed can be dictated by an external controller and must provide enough torque to induce the desired acceleration on the heaviest user. The shafts must be resistant to fatigue failure and sized based on maximum belt tension and motor output. The belts must be selected based on the force required to induce the highest intensity perturbation on the heaviest user. See the relevant detailed design chapters in the Appendix for more information.

The PPT should be operated by a single individual and require no coding experience. The operator needs to control belt speed and perturbation intensity from an external Human-Machine-Interface (HMI) (Appendix G). The total price of the system also needs to be comparable to existing research units to be accessible for clinical and academic teams (Appendix J).

Verification of functional requirements utilized an experimental test. A human analog, constructed from a 132 kg weighted bag, was used to simulate both the rotational and translational momentum of a participant during perturbation. A step input to maximum speed, then a hard stop was implemented to create the highest stress condition. Starting at zero initial velocity, the belt was accelerated at 12 m/s^2 for 0.3 seconds and then immediately decelerated back to zero at the same rate. The test was performed ten times, and slow-motion video was recorded to investigate relative motion between the belt and drum, which was used to determine if adequate pretension had been applied to the belts. After the test the PPT was disassembled, and all components were inspected for premature wear and damage. Specifically, the critical loading components were examined; shafts were inspected for hairline fractures using a liquid die penetrant system (Magnaflux, Glenview, IL, USA), belts were visually examined for tears and delamination of the splice, and bearings were examined for excessive runout and resistance-free rotation. For more information about device validation, see Appendix I.

Portability

The PPT is intended as a portable research and clinical tool that travels to multiple locations and can be set up by two operators. A pickup truck is readily available to most research and clinical teams in the United States. The PPT must fit between the wheel arches with the gate closed, requiring a maximum size of 1.1m x 1.9m (44" x 78") [28, 29]. The device must be safely transported from the truck to the testing location. The maximum safe lifting force for a two-person lift is 80kg (176 lbs) [30]. See Appendix F for more information.

The PPT must run on standard household power within the United States without tripping a breaker or creating a fire risk. For 120-volt systems, the maximum current draw can not exceed 15 amps or 50 amps when connected to 240.

Perturbation Response Testing

An experimental human study was performed to verify that the treadmill elicits postural responses analogous to trips and slips. A single participant consented to an Institutional Review Board approved protocol. Starting at zero initial velocity, the belts were accelerated at 12 m/s^2 for 0.3 seconds and then decelerated back to zero over eight seconds. The test was performed ten times, and body segment kinematic data were collected (Xsens, El Segundo, CA, USA) to estimate maximum trunk deflection and compare it to known postural responses [21-23]. Motor diagnostic data were collected using software supplied by the manufacturer (ClearPath, Teknic, Victor, NJ, USA) to assess torque utilization and motor performance. Following the postural testing, the treadmill was again disassembled and examined for signs of excessive wear. See Appendix I for more information.

RESULTS

Figure 4. Images of Completed Treadmill. The black frame shown in the middle and right pictures was used to prevent user injury while the treadmill was in use during the clinical tral. This was accomplished via a climbing harness attached to the frame.

Functional Requirements

System Overview

Each belt of the split-belt treadmill (Fig. 4) is connected to a dedicated motor (Fig. 5A) (CPM-MCVC-N0563P-RLN, Teknic, Victor, NJ, USA) via a timing belt and pulley with a 5.6:1 gear ratio. Each motor can output a peak torque of 32.9 N-m (24.3 ft-lb). The shafts connecting the pulley and drums are sized based on locations of interest (Fig. 6), where the outer diameter varies based on maximum internal stresses. Each belt is 0.46 m (18") wide, and the gap between the belts is 1 cm (0.375"). Initial device testing showed that the motors would shut down during hard deceleration periods. When the motors are resisting the motion of a load, they act as generators, feeding voltage back into the system. The selected motors have circuitry to deal with this, but it can easily become overwhelmed with high inertia loads. To solve this issue, a breaking resistor (RES 255, Teknic, Victor, NJ, USA) was installed, which converts excess energy into heat (Fig. 5B). This solved the problem, and no overvoltage faults were observed after this addition.

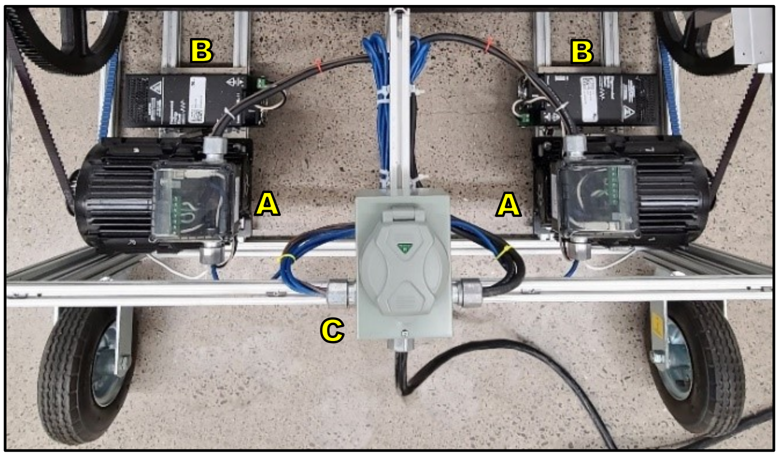

Figure 5. Front of Treadmill Showing Electrical Components. (A) Motors used to drive the belts. (B) The breaking resistors used to dissipate excess mortor energy as heat. (C) The power input box used to supply external power to the treadmill.

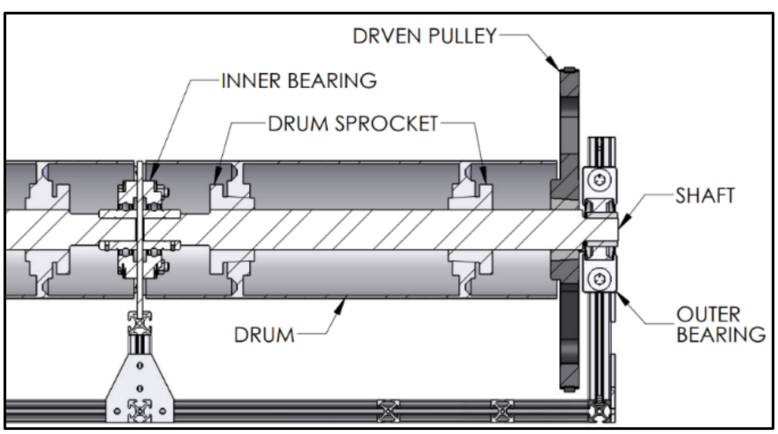

Figure 6. Shaft Component Diagram. The outer diameter of the shaft is determined by calculating maximum stresses at locations of interest.

Figure 7. Final Configuration of the Controller Module. Top-down view showing the buttons, switches, and indicator lights used to control the treadmill.

<u>Motor Control & System Cost</u>

The HMI (Fig. 7) has five inputs that can be used to control the PPT. A rotary switch dictates the desired perturbation intensity from predefined values. A center detent potentiometer controls the steady-state walking speed for walking perturbations and provides tactile feedback when the belt speed is set to zero. A three-position switch determines which belt will be active (left, right, or both). A pushbutton switch initiates the perturbation, providing tactile and auditory feedback when engaged. A green trigger status Light Emitting Diode (LED) indicates when a perturbation is being performed. A large Emergency Stop button shuts down the treadmill in case of an emergency with a red LED to indicate activation. A green LED on the right indicates when the system is active and awaiting operator input. All LEDs blink in unison if the software detects a dangerous situation, such as when the belt speed is at a non-zero value on initial power-up or when the Emergency Stop is disengaged. See Appendix G for more information. The treadmill is controlled with an Arduino Mega 2560 microcontroller (Arduino, Somerville, MA, USA), which monitors HMI button states and regulates motor speed via Pulse Width Modulated (PWM) signals. Predetermined perturbation profiles are stored in memory via an array of speeds (PWM values) and incremental timing values.

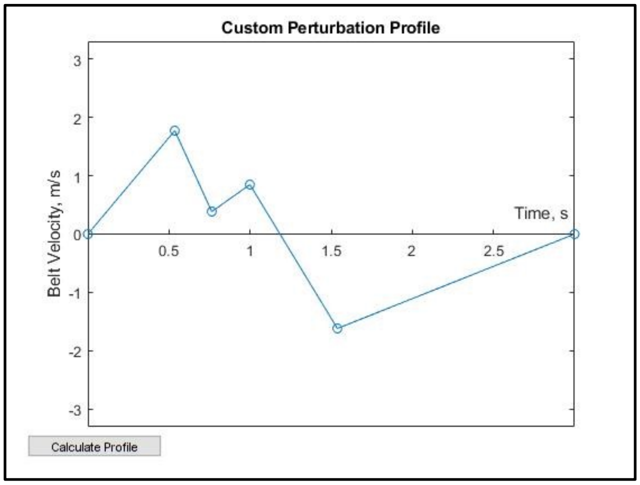

Figure 8. Matlab GUI for Creating Custom Perturbation Profiles. Points (blue circles) are dragged to appropriate locations and the motor speed is calculated by interpolating the line between points.

Custom perturbation profiles are created via a Matlab (Mathworks, Natick, MA) Graphical User Interface (GUI), where profiles of belt speed vs. time are indicated with mouse click events by dragging points to appropriate locations (Fig. 8). The software interpolates the line between points and calculates the appropriate PWM and timing values. The resulting array is saved as a CSV file that the Arduino can read. This approach requires no coding experience, as contextual menus and popups are used to define initial parameters, while also simplifying the creation of large, complex profiles. See Appendix H for more information on software design. The system's total cost, including all accessories, was approximately $11,000. For more component cost information, see Appendix J.

Verification of Performance

After the human analog test, no abnormalities were detected when disassembling the treadmill and examining critical loading components. No hairline fractures were observed in the shafts, the belt splice was intact, and the bearing showed no signs of excessive wear.

Portability

Transport of the treadmill is facilitated by wheels in the front and handles in the back (Fig. 9). Its outer dimensions are 1 m x 1.8 m (43” x 72”). The usable walking area is 1.67 m x 0.92 m (66” x 36.375”). The treadmill weighs approximately 181 kg (400 lbs) when fully assembled. The frame was made from aluminum T-Slot sections to facilitate portability and reduce overall mass. A two-ply fabric treadmill belt was selected for its strength and low weight [31].

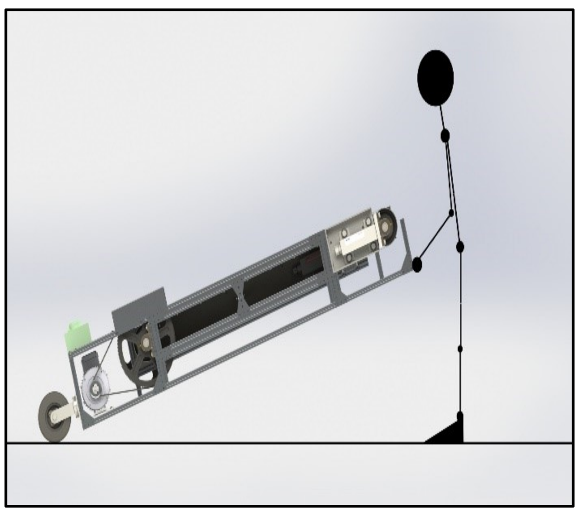

Figure 9. Manual Treadmill Transport. The treadmill is manually transported like a wheelbarrow with handles in the back and wheels in the front.

The motors can operate with either 120/240-volt input, which enables a top speed of 1.6/3.3 m/s (3.5/8.1 mph). When connected to 120-volts, the treadmill can draw up to 17 amps, which will trip a standard residential 15-amp breaker. Many of the intended locations do not have an available 240-volt source. Therefore, a 13,000-watt generator was selected (XP13000EH, DuroPower, Covina, CA, USA), facilitating maximum perturbation intensity in any location. The generator can output 50 amps on the 240-volt line and can run on gasoline or propane [32]. A 15.25 m (50’) 6 AWG extension cord delivers power from the generator to the treadmill, allowing the generator to be placed outside, reducing noise and noxious fume concerns. The extension cord connects to a power input box on the treadmill (Fig. 5C), which also serves as a connection point for the motor control wiring harness. A 3 m (10’) data cable connects the HMI to the treadmill, with connectors at each end to aid in transport and disassembly. This allows for remote operation by a single operator from a central location.

Perturbation Response Testing

Motion capture data from the human subject test (Fig. 10) showed a mean, maximum trunk flection angle of 26.9°, similar to the results of previous studies [21-23]. The motor diagnostic software showed a peak torque utilization of 40%. Following the postural testing, disassembly of the treadmill found no signs of excessive wear.

Figure 10. Setup for Human Subject Test.

DISCUSSION

Perturbation Balance Training is an effective method to reduce fall rates in older adults. Current devices are large, expensive, and generally inaccessible. This presents a barrier to implementing PBT, especially for older adults with limited mobility or those in rural/remote areas. Therefore, there is a clear need to develop a low-cost and accessible training solution.

The objective of this project was to design, fabricate, and validate a Portable Perturbation Treadmill. The project was split into three main requirements: functionality, portability, and postural response verification.

Functional Requirements

The treadmill needed to be dual-belt, accommodate a user of up to 118 kg and provide a belt acceleration of up to 12 m/s^2. In addition to satisfying mechanical loading requirements, two 0.46 m (18") wide belts were selected for a second reason. It is the recommended minimum width for a traditional, single-belt treadmill [33-35]. Since each side of the dual-belt treadmill was designed to be redundant (each belt, drivetrain, and motor can handle 100% of the load), it is possible to fabricate two single-belt treadmills from existing components with little additional cost.

A single individual with no programming experience can operate the treadmill because the HMI uses buttons and switches to dictate perturbation parameters, and the Drag & Drop Perturbation Profile Generator uses contextual menus and prompts to create new perturbation profiles. While there is no maximum on the number of draggable points, the practical maximum is around 20 due to the size of each point on the screen and the lack of a scrollable graph. The software is not limited to linear perturbations. Approximations to nonlinear functions can also be used (parabolic, sawtooth, trigonometric, etc.). The motor control software was initially designed to calculate belt speed profiles independently whenever an HMI button or switch changed state without an external computer. Initial device testing showed that the Arduino lacked sufficient memory for internally calculated profiles longer than two seconds because the profile creation function requires significant memory recourses. The limitations of the Arduino could be overcome with a more powerful microcontroller, such as a Teensy or Raspberry Pi. Other devices commonly used in perturbation training range in price from \$50,000 to \$150,000. The total cost of the PPT was less than \$11,000, representing a 75% cost savings. Therefore, any clinic could potentially purchase this for their use, and the cost requirements have been satisfied. Further cost reductions could be achieved if the design was modified to use a single belt, ordering components in larger quantities, and eliminating the generator for locations with adequate power sources. With these modifications, the total cost would be approximately \$4,000 per unit.

The results of the human analog test show that the treadmill is safe to use with a user of up to 118 kg and a maximum 12 m/s^2 belt acceleration. However, higher accelerations are possible for users of lower weight. The results of the clinical trial further reinforce the safety of the treadmill. It was used for 28 days at multiple test sites for approximately five hours each day, and no component failures were observed. Therefore, the functional requirements of the treadmill have been satisfied.

Portability

With outer dimensions of 1 m x 1.8 m (43” x 72”), the treadmill fits within a standard pickup truck bed. Therefore, the dimensional requirements are satisfied. There was one aspect where the device did not meet the project goals. The weight of the system exceeded initial expectations. The treadmill weighs 181 kg (400 lbs) with a centrally located center of mass, meaning that the operators need to lift approximately 91 kg (200 lbs) when moving the treadmill. This does not meet OSHA standards for a two-person lift; therefore, we recommend that a team of at least three people is used to move the device. Half of the overall weight is from drivetrain components such as the pulleys, shafts, and drums, which are made from solid steel or cast iron. However, the design could be modified to use lightweight materials with an estimated weight reduction of approximately 50 kg (110 lbs). Additionally, if a dual belt system was not needed, the total weight would be approximately 70 kg (150 lbs) which would be in line with OSHA regulations. The treadmill was used for 28 testing days in the clinical trial and transported to and from the testing site each day, reinforcing that portability was achieved even though the weight requirements were not met.

Perturbation Response Testing

The primary goal of this project was creating the perturbation treadmill, which includes testing that it produces perturbations simulating trips and slips. Previous studies have indicated that a trunk flection angle of approximately 25° simulates real-world slips and trips, we achieved 26.9°, therefore the postural response requirements have been satisfied. As a measure of safety, the Perturbation Response Test was performed on a healthy young adult. During the clinical trial, many older adults could not successfully recover from the high-intensity profile used in this test, demonstrating that the treadmill exceeded the postural response requirements for individuals in the target population. Further testing is needed to identify the range of postural responses from this system.

CONCLUSION

This work outlined the design and validation of a portable, split-belt perturbation treadmill. The system allows for a belt acceleration of 12 m/s^2 on a user up to 118 kg with independent belt control. It weighs 181 kg and is moved like a wheelbarrow with wheels in the front and handles in the back. High-intensity perturbations can be performed at any location, and the system requires no coding experience to operate. It costs 75% less than similar commercial devices, is capable of producing postural responses similar to slips and trips, and was used in multiple locations in a clinical trial.

APPENDICES

APPENDIX A:

INDUSTRY DESIGN GUIDELINES

What is a Treadmill Belt?

Treadmill belts are a subset of conveyor belts, and both are typically manufactured in the same facilities [36]. The main difference between the two is that treadmill belts have a fabric backing allowing them to be lightweight, flexible, and strong. Conveyor belts are typically made from rubber or other highly durable materials, with steel cords providing the strength [37].

The Conveyor Belt Manufacturers Association (CEMA) publishes literature regarding the design of conveying systems in aspects such as system configuration, load handling capabilities, and belt width [38]. The underlying mathematics of the CEMA standards were used as a reference for the design process of the treadmill, but their procedure was not strictly adhered to. This is because the calculations they use make a variety of simplifications and assumptions which were not suitable for this project, generally relating to the assumption of a thick rubber conveyor belt.

Conveyor Belt Tracking

Conveyor belt tracking is the process of aligning and controlling a conveyor belt so that it stays on the correct path [39]. Multiple factors contribute to tracking accuracy, including belt design, loading characteristics, and system configuration. Inadequate tracking can result in the destruction of the belt and poor performance of the system.

The most significant factor in belt tracking is the parallelism of the drums and other components that contact the belt [40]. The drums and rollers must be installed at right angles to the belt running axis. Misalignment of these components will result in a net steering effect, causing the belts to drift away from the center of the pulleys (Fig. 11L). This is because flat belts have a natural tendency to track towards the side with the lowest tension [41].

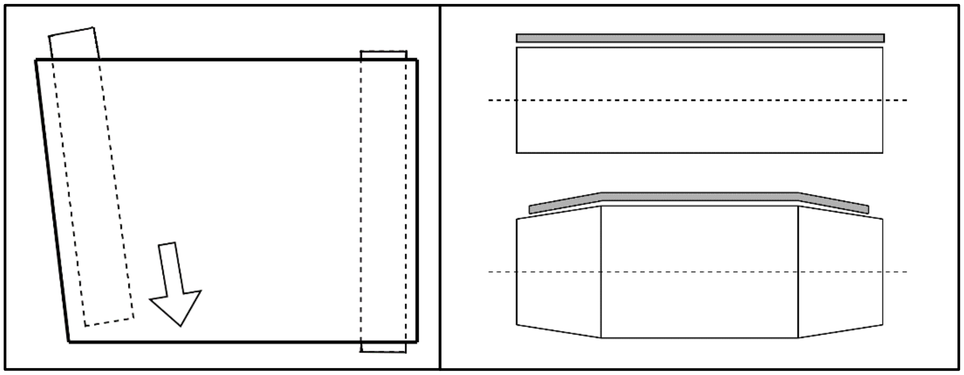

Figure 11. Belt Tracking. Left. Misalligined Belt. The belt will naturally track towards the side with the least tension. Right. Types of Conveyor Belt Drums. Flat drums and Crowned drums are comonly used in convyors.

There are two types of conveyor belt drums used in industry. They are flat and crowned drums (Fig. 11R). A flat drum has a flat and featureless surface. This type of drum does not assist in belt tracking. A crowned drum has a convex, conical shape that is higher in the center than the edges. This causes an imbalance in the forces within the belt and results in a natural self-centering action [42]. Most industry guidelines recommend crowned pulleys as the primary tracking method [38, 41]. Using a crowned pulley requires specific design criteria, notably the drum must be wider than the belt. The typical recommendation is that the drums are 1” or 10% wider than the belt, whichever is greater [38, 41]. This is so the belt has room to deviate from the center and does not lose contact with the surface of the drum.

Flat pulleys have no intrinsic effect on belt tracking. Lateral loads such as those commonly seen during gait would cause the belts to misalign if other provisions were not taken. The Habasit Fabric Conveyor Belt Engineering Guide suggests that lateral guides can be used as a secondary belt tracking measure [41]. Lateral guides are constructed from low friction materials and prevent lateral movement by a slot in the guide (Fig. 12). The downside of using lateral guides is that they increase belt edge wear, and are themselves a wearing component, therefore they are not commonly used in industry [41]. Tracking belts using lateral guides only works when the guide is placed close to where the belt contacts the pulley and are specific to a direction of travel. This is because any corrections to tracking need to happen before the belt contacts the drum [41].

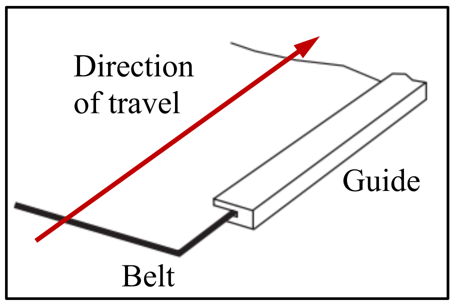

Figure 12. Lateral Guide Example. The belt is prevented from moving laterally by rubbing against the edge of the slot in the guide.

Belt Tension

The role of friction in the equilibrium of ropes wrapped around shafts was analyzed by Euler [43]. He presented the well-known capstan formula, which relates the slack and tight tensions of a rope to the friction coefficient and angle of wrap of the rope on the pulley.

$$F_1 = F_2 \times e^{(\mu\theta)}$$

F_1 is the tension on the tight side, F_2 is the tension on the slack side, μ is the coefficient of friction between the two surfaces, and θ is the contact angle between the belt and pulley expressed in radians (Fig. 13). This equation was first applied to flat belts by Eytelwein, and is commonly known as the Euler-Eytelwein Formula [44, 45].

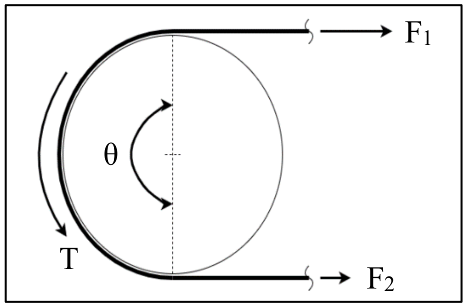

Figure 13. Free Body Diagram of Belt Tension.For the torque applied in the direction shown by T, F_1 is the tension in the tight side, F_2 is the tension in the slack side, θ is the angle of wrap.

Shortcomings of Euler- Eytelwein Formula

Modern research suggests some shortcomings of the Euler-Eytelwein Formula. As the belt travels over the pulley from the tight to the slack side, the tension in the belt changes from T_1 to T_2. A study by Brett DeVries determined that the coefficient of friction has a strong dependence on contact pressure [46]. Although he could not solve the equations for a pressure-dependent coefficient of friction analytically, a best-fit approximation from experimental data was proposed. The frictional force is traditionally calculated by multiplying the coefficient of friction by the normal force. Since the normal force is distributed over the apparent contact area, it could be expressed as pressure. Thus, pressure multiplied by the coefficient of friction is the frictional force per unit area, also known as shear stress. They created a set of graphs using experimental data that depict maximum shear stress as a function of belt pressure at impending slip. Using these graphs and an equation that relates shear stress and effective tension, the factor of safety for the maximum shear stress available to prevent slip can be calculated. This equation has the form:

$$\tau_e = \frac{2T_e}{\varphi D(BW)}$$

Where τ_e is the effective shear stress, T_e is the effective tension, φ is the angle of wrap expressed in radians, D is the diameter of the pulley, and BW is the belt width. This methodology quantified two intuitive concepts. First, there is an upper limit to the coefficient of friction, and second, larger diameter pulleys are capable of more traction [46].

Belt Creep

Conveyor belts are not rigid structures. When subjected to an applied load, they will elongate by some quantifiable amount. This creates a problem in calculating the contact area between the belt and the pulley. As the belt travels from the tight to the slack side, the belt will change in length due to differential tension. This creates an area of slip between the two segments. This change in length is time-dependent and is known as creep. This theory was first proposed by Gasthof [47]. It states that the arc of contact between the belt and the pulley will undergo two regimes, a slip zone at the exit region and a stick zone over the remaining arc of contact. These models have recently been improved by considering the effects of blet stiffness, inertia, and radial compliance [48].

APPENDIX B:

DETAILED MOTOR & PULLEY CALCULATIONS

Introduction

Motor and pulley selection are highly dependent in nature. An appropriate motor can not be found unless the final gear ratio from the pulley is known, and the gear ratio from the pulley can not be determined unless the motor torque and speed are known. Selecting appropriate components requires an iterative approach, where both must work together in unison. It is for this reason that values from the selected motor are used in the pulley selection calculations and vice versa.

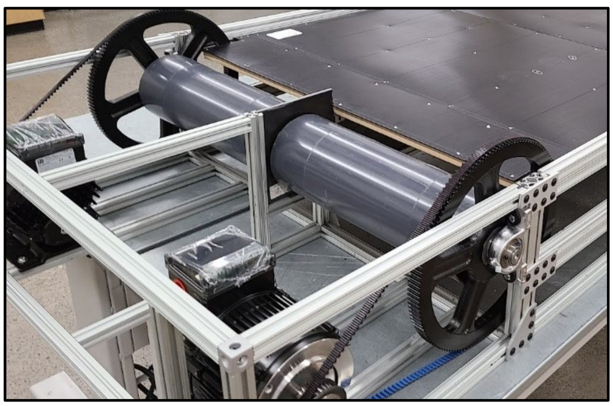

Figure 14. Front of Treadmill Showing Motors, Pulleys, & Timing Belts

Analysis Setup

Two types of motion will occur simultaneously when a perturbation is triggered (Fig. 15L). There is a rotational component, as in the user tends to rotate around their center of mass, and a translational component, as in the user will be pulled horizontally along the treadmill. The exact magnitudes of each can not be determined in advance since they are dependent on foot placement and an individual's body morphology. Therefore, the following analysis will consider a worst-case scenario where the user is rotating and translating at the maximum prescribed rate. It should be noted that this is an overestimate as a rigid body approximation is used. Realistically, human bodies are compliant, and joints will bend under load.

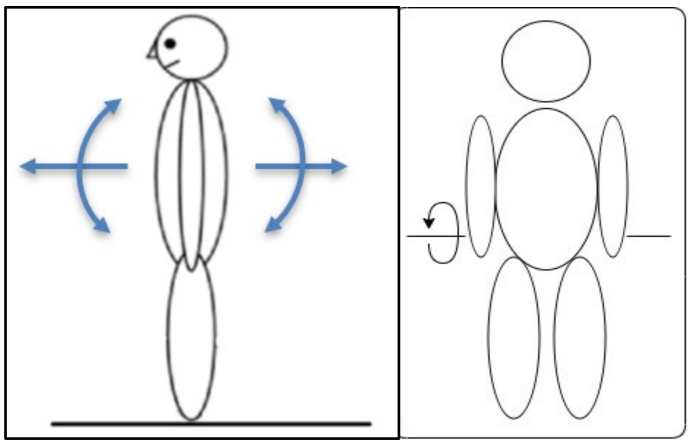

Figure 15. Body Movement Diagrams. Left. Rotational and translational motion occurs when a perturbation is performed. Right. Frontal plane rotation about the body's center of mass.

User Information and Design Values

Since the user's motion has a rotational component, mass moments of inertia must be determined. This is because the belts accelerating under the user will tend to cause a rotation about the body’s center of mass in the frontal plane (Fig. 15R), and the mass moment of inertia is required to calculate torque. This value was found to be $12\ kg\ m^2$ [49, 50] using data from the CDC and Department of Defense for an adult male standing upright, with the arms at the sides.

A 70-79 adult male was selected as the target demographic due to the increased fall risk and data availability. A summary of the user data can be seen in Table 1. The CDC lists the average weight and height of a 70 to 79-year-old male, in the 95th percentile, as 262 lbs. (118 kg) and 67.4 in (1.71 m), respectively [24, 51].

Gender	Male
Race	All race and Hispanic-origin groups
Weight	292 lbs (118 kg) [24]
Height	67.4 in (1.71 m) [51]
Mass moment of inertia about frontal axis	23.7 $lb\ ft^2$ (12 $kg\ m^2$) [49, 50]

Table 1. Summary of User Demographic Information.

The maximum belt acceleration needed to be determined as it would affect the selection of other components, such as the motors and shafts. This value needed to be large to achieve the desired perturbation intensity while small to reduce the size of drivetrain components and overall weight. This presented a problem because there is no broadly accepted value, and the accelerations used in current literature can range from 3 m/s^2 to 15 m/s^2 [25-27]. After consulting with the project advisor, a maximum belt acceleration of 12 m/s^2 was selected to accommodate a wide range of uses while minimizing overall weight and design complexity.

Drum Selection

Crowned drums could not be used due to the additional width requirement, as outlined in Appendix A, and the desire to keep the distance between the two treadmill belts small. A 6" diameter flat drum was selected, and secondary belt tracking measures were used. This included the installation of belt guides. The guides are a wearing component and cause belt edge wear, but due to the treadmill belts' low cost and the infrequency of use, this was deemed an acceptable compromise. With forward and reverse operation anticipated, multiple guides were needed because corrections to belt tracking must occur before the belt contacts the drum. For more information about belt tracking, see Appendix F.

Drive Belt and Gearing Selection

Due to the iterative nature of design, the Gates Design Flex Pro software was used to select an appropriate synchronous timing belt and pulley [52]. The benefit of using this software, as opposed to manual calculations, is that it will give a range of acceptable belt and pulley combinations, with cost estimates and specific model numbers. The inputs to the software are listed in Table 2. The driving pulley torque listed is the maximum torque output available from the motor. A service factor of 1.3 was selected based on recommendations from the manufacturer for an electric motor with intermittent use, driving a load with moderate shock. The software's output with details of the selected drive units can be seen in Appendix J.

Input Parameter	**Value**
Driving Pulley Speed	825 RPM
Driving Pulley Torque	24.5 ft-lb.
Driving Pulley Shaft Diameter	0.625 in.
Driven Pulley Speed	150 RPM ±5%
Driven Pulley Shaft Diameter	1.75 in.
Center-to-Center Distance	14 in. ±10%
Desired Gear Ratio	5.5:1 Down
Power Source	Electric Motor
Service Factor	1.3
Desired Product Line	Poly Chain GT Carbon
Bushing Type	Taper-Lock

Table 2. Inputs to Timing Belt Selection Software.

The software recommended a 12-millimeter-wide timing belt with an 8-millimeter pitch, a 25-tooth driving pulley, and a 140-tooth driven pulley. The final drive ratio was then 5.6:1, which was deemed adequate based on available motor torque and speed. The recommended belt was checked using a horsepower rating table supplied by the Gates Corporation for the 8mm GT Carbon belt [53]. It was found that at an input speed of 870 RPM and a driving pulley with 25 teeth, the belts were rated for up to 8.26 horsepower. The selected motor has a maximum power of 7.75 horsepower on 240 volts, so the results of the software were deemed valid.

<u>Motor Selection</u>

The goal of this calculation was to find an equivalent mass moment of inertia about the motor's hub using a reflected load inertia approach [54]. Once this value was found, the required torque was calculated using Newton's Second Law. Inertial factors from all loads accelerated by the motor were considered, including rotating and translating components (Fig. 16). First, the kinetic energy for rotating objects was determined. Next, the kinetic energy for translating objects was determined. Finally, the two are summed, and an equivalent mass moment of inertia was calculated. Mass and inertia values for individual components are listed in Table 3.

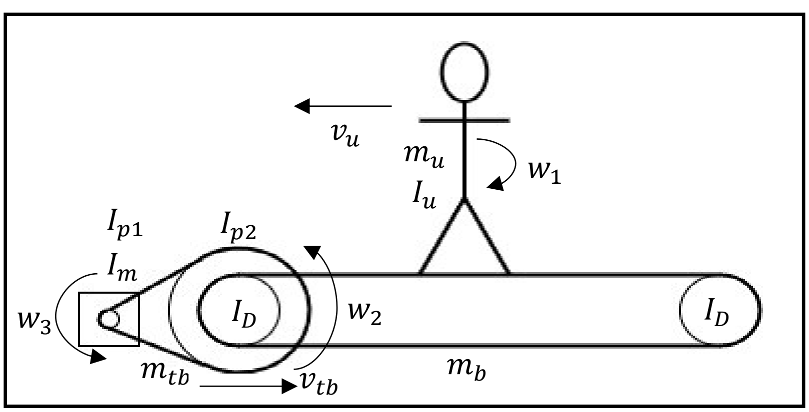

Figure 16. Variables for Load Inertia Calculations. Variables m_u, m_b, and m_{tb} represent the mass of the user, treadmill belt, and timing belt. I_u, I_D, I_{p2}, I_{p1}, and I_m represent the moment of inertia for the user, drum, driven pulley, driving pulley, and motor. w_1, w_2, and w_3 represent the rotational velocities for the user, drum, and motor. v_u and v_{tb} represent the linear velocities of the user and timing belts.

Item	Symbol	Value
User	m_u	$119\ kg$
	I_u	$12\ kg\ m^2$
Timing Belt	m_{tb}	$0.4626\ kg$
Treadmill Belt	m_b	$3.47\ kg$
Drum	I_D	$0.041833\ kg\ m^2$
Driven Pulley	I_{p2}	$0.138179\ kg\ m^2$
Driving Pulley	I_{p1}	$0.000104\ kg\ m^2$
Motor	I_m	$0.0019\ kg\ m^2$

Table 3. Summary of Masses and Moments of Inertia. It should be noted that the moment of inertia for the rotating components should include all items fixed to that device, such as any shafts or couplings. The values for drum, motor, driven, and driving pulleys, come from data provided by their respective manufacturers. For more information, see Appendix J

Kinetic Energy of Objects in Rotational Motion. The total kinetic energy for all rotating components can be found by summing the individual components.

$$KE_{rot} = \sum KE_{individual}$$
$$KE_{rot} = KE_u + KE_d + KE_{p2} + KE_{p1} + KE_m$$

The formula for the kinetic energy of rotating objects is shown below.

$$KE = \frac{1}{2}\, I\, w^2$$

Where KE is the kinetic energy, I is the mass moment of inertia, and w is the rotational velocity. We will break the next stage into multiple groups based on objects moving at the same rate. For example, the drums and driven pulley rotate at the same rate because they are connected to the same shaft. This is an important distinction to make. Otherwise it would imply that the motor is spinning as fast as the user, which is not the case.

There are three distinct rotational velocities that govern the dynamics of the system. The first group is objects moving at the same rate as the user. The user is the only contributor to this group. The second group includes the drums and driven pulley. The third group consists of the driving pulley and motor.

$$KE_1 = \frac{1}{2} I_u \, w_1^{\ 2}$$
$$KE_2 = I_d \, w_2^{\ 2} + \frac{1}{2} I_{p2} \, w_2^{\ 2}$$
$$KE_3 = \frac{1}{2} I_{p1} \, w_3^{\ 2} + \frac{1}{2} I_m \, w_3^{\ 2}$$

It should be noted that the ½ factor for the drum in KE_2 was eliminated because there are two drums (one in the front and one in the back). Combining these equations, we arrive at the total kinetic energy for the rotating components.

$$KE_{rot} = \frac{1}{2} I_u \, w_1^{\ 2} + I_d \, w_2^{\ 2} + \frac{1}{2} I_{p2} \, w_2^{\ 2} + \frac{1}{2} I_{p1} \, w_3^{\ 2} + \frac{1}{2} I_m \, w_3^{\ 2}$$

In order to simplify this equation further, we need to find the ratios of relative velocities and express them in terms of a single common variable. This is accomplished by examining the linear velocities at the point of contact, which must be the same. For example, the velocity of the user must be the same as the velocity of the belts (as governed by the rotational speed of the drum and its radius).

$$v_u = r_d \, w_2 = r_u \, w_1$$

Solving for w_1 and adding in known values, we arrive at the following formula.

$$w_1 = \frac{r_d \, w_2}{r_u} = \frac{0.0762m \, * \, w_2}{0.961m}$$
$$w_1 = 0.07929 \, w_2$$

The same procedure can be applied for the ratio of w_2 to w_3. It should be noted that we are using the radius of the pitch circle for the driven and driving pulleys since this is the mean point of contact with the timing belt.

$$v_{tb} = r_{p2}\, w_2 = r_{p1}\, w_3$$
$$w_2 = \frac{r_{p1}\, w_3}{r_{p2}} = \frac{0.03182m * w_3}{0.1783m}$$
$$w_2 = 0.1785\, w_3$$

Making these substitutions into KE_{rot} we arrive at the following:

$$KE_{rot} = \frac{1}{2} I_u\, (0.07929\, w_2)^2 + I_d\, {w_2}^2 + \frac{1}{2} I_{p2}\, {w_2}^2 + \frac{1}{2} I_{p1}\, {w_3}^2 + \frac{1}{2} I_m\, {w_3}^2$$
$$KE_{rot} = \frac{1}{2} I_u (0.07929 * 0.1785\, w_3)^2 + I_d (0.1785\, w_3)^2 + \frac{1}{2} I_{p2} (0.1785\, w_3)^2 + \frac{1}{2} I_{p1}\, {w_3}^2 + \frac{1}{2} I_m\, {w_3}^2$$
$$KE_{rot} = \frac{1}{2} I_u (0.0141\, w_3)^2 + I_d (0.1785\, w_3)^2 + \frac{1}{2} I_{p2} (0.1785\, w_3)^2 + \frac{1}{2} I_{p1}\, {w_3}^2 + \frac{1}{2} I_m\, {w_3}^2$$

Kinetic Energy of Objects in Translational Motion. We will follow the same procedure as the previous calculations. The translational kinetic energy is essential to include because the user's translational mass dramatically impacts the total torque required.

$$KE_{lin} = \frac{1}{2} m_u\, {v_u}^2 + \frac{1}{2} m_b\, {v_u}^2 + \frac{1}{2} m_{tb}\, {v_{tb}}^2$$

Next, the ratio of v_u to v_{tb} was found to combine equations.

$$v_{tb} = \frac{v_u\, r_{p2}}{r_d} = \frac{0.1783m * v_u}{0.0762m}$$
$$v_{tb} = 2.3438\, v_u$$
$$KE_{lin} = \frac{1}{2} m_u\, {v_u}^2 + \frac{1}{2} m_b\, {v_u}^2 + \frac{1}{2} m_{tb}\, (2.3438\, v_u)^2$$

Before we can combine KE_{rot} and KE_{lin} we need to convert the linear velocity of the user to rotational velocity.

$$v_u = r_d * w_2 = 0.0762\, w_2$$
$$KE_{lin} = \frac{1}{2} m_u\, (0.0762\, w_2)^2 + \frac{1}{2} m_b\, (0.0762\, w_2)^2 + \frac{1}{2} m_{tb}\, (2.3438 * 0.0762\, w_2)^2$$

Next, we substitute in the ratio of w_2 to w_3 to get a single common variable.

$$KE_{lin} = \frac{1}{2}m_u\,(0.0762 * 0.1785\,w_3)^2 + \frac{1}{2}m_b\,(0.0762 * 0.1785\,w_3)^2 + \frac{1}{2}m_{tb}\,(2.3438 * 0.0762 * 0.1785\,w_3)^2$$

$$KE_{lin} = \frac{1}{2}m_u\,(0.0136\,w_3)^2 + \frac{1}{2}m_b\,(0.0136\,w_3)^2 + \frac{1}{2}m_{tb}\,(0.0318\,w_3)^2$$

<u>Torque and Total Kinetic Energy.</u> Combining KE_{rot} and KE_{lin} we arrive at the following:

$$KE_{comb} = KE_{rot} + KE_{lin}$$

$$KE_{comb} = \frac{1}{2}I_u(0.0141\,w_3)^2 + I_d(0.1785\,w_3)^2 + \frac{1}{2}I_{p2}(0.1785\,w_3)^2 + \frac{1}{2}I_{p1}\,{w_3}^2 + \frac{1}{2}I_m\,{w_3}^2 + \frac{1}{2}m_u\,(0.0136\,w_3)^2 + \frac{1}{2}m_b\,(0.0136\,w_3)^2 + \frac{1}{2}m_{tb}\,(0.0318\,w_3)^2$$

We can now substitute in known values and simplify.

$$KE_{comb} = \frac{1}{2}12(0.0141\,w_3)^2 + 0.041827(0.1785\,w_3)^2 + \frac{1}{2}0.138179(0.1785\,w_3)^2 + \frac{1}{2}0.000104\,{w_3}^2 + \frac{1}{2}0.0019\,{w_3}^2 + \frac{1}{2}119\,(0.0136\,w_3)^2 + \frac{1}{2}3.47\,(0.0136\,w_3)^2 + \frac{1}{2}0.4626\,(0.0318\,w_3)^2$$

$$KE_{comb} = \frac{1}{2}\;0.0172907\,{w_3}^2$$

Thus, the equivalent mass moment of inertia of the system was found to be 0.0172907 kg m^2. Before the required torque could be calculated, it was necessary to determine the angular acceleration of the motor. Assuming a peak perturbation velocity of 1.2 m/s, a 6" diameter drum, and a 5.6:1 gear ratio, this would equate to a motor acceleration of 881.86 $\frac{rad}{s^2}$. Using Newton's Second Law and making the appropriate substitutions, we arrive at the motor torque required to achieve the desired acceleration for the specified worst-case scenario.

$$\alpha = 157.4803 * 5.6 = 881.86\,\frac{rad}{s^2}$$

$$T = I\,\alpha\ = 0.0172907 * 881.86$$
$$T = 30.5\ Nm$$

Selected Motor Features

Using the data previously calculated, an AC brushless servomotor was selected from the Teknic catalog. They are a company known for making hybrid stepper and servo motors, and these specific motors are often used in motion control applications, such as CNC machines. The motor specifications can be seen in Table 4 for single phase 120-volts and split phase 240-volts. This specific model and manufacturer was chosen because it was the most affordable option, could run on various input voltages, and could be controlled in multiple ways. Additionally, Teknic provides a Windows application for monitoring motor parameters in real-time.

Model	CPM-MCVC-N0563P-RLN	
	Input Voltage	
	120 VAC	240 VAC
Peak Torque [47]	23.7 ft-lb (32.9 N-m)	23.7 ft-lb (32.9 N-m)
Continuous Torque [47]	6 ft-lb (8.1 N-m)	6 ft-lb (8.1 N-m)
Max Speed [47]	1010 RPM	2410 RPM
Peak Power [47]	2.39 hp (1,779 W)	6.77 hp (5,045 W)
Continuous Power	0.97 hp (725 W)	1.86 hp (1,384 W)

Table 4. Details of the Selected Motor.

Motor Control Methods

The motors can be controlled in several ways (for more information, please see the user manual) [55]. The specific operating mode that was used is known as "follow digital velocity with bidirectional PWM input". In this mode, the motors receive a PWM signal whose duty cycle is proportional to the desired motor speed. It is bidirectional because the speed can be controlled in either direction. More specifically, a duty cycle of 0% would command the motors to spin clockwise at the maximum permittable speed, while a duty cycle of 100% would command the motors to spin at maximum speed in the counterclockwise direction. A duty cycle of approximately 50% commands the motor to stop. The maximum permittable speed is based on the motor's input voltage.

APPENDIX C:

DETAILED BELT TENSION CALCULATIONS

Dimensional Considerations & Analysis Setup

Multiple online sources recommend a minimum belt width of 18” and a minimum useable length of 5’ [33-35]. With 6” drums, this would give a total useable length of 138.85”. Since treadmill belts are only sold in whole number increments, a total belt length of 140” was selected. This resulted in a total distance of 60.5” between centers, which was deemed acceptable. The required belt width was determined by the belt tension calculations in the following sections. In those calculations, we assumed a worst-case scenario of the entire load being applied to a single belt of our dual belt design (the user is standing with both feet on a single belt when a perturbation is performed). This assumption makes the left and right systems redundant, where each side can handle 100% of the load independently.

Calculating Minimum Belt Width

The belts were sized in accordance with the maximum torque output of the motor. This was done to ensure that the belts would not be the weak point in the system and that the motors would not be able to tear apart the belts. If an overload condition were encountered, the motors would be unable to provide enough power, saving the belts and related drivetrain components. For more information on the mechanical properties of the treadmill belts, see Appendix J. The calculations in the following section will determine the narrowest belt capable of withstanding the load.

The following process was based on suggestions from Shigley’s Mechanical Engineering Design [54]. The manufacturer lists the mass of the belt as $2.3\ \frac{kg}{m^2}$ [31]. Multiplying this by an unknown belt width, b, we get $\gamma = 2.3\ b\frac{kg}{m}$. Next, the centrifugal force was calculated from the belt as it rotates around the drum. For this step, the velocity of the belt, V, was $1.2\frac{m}{s}$, the same as in a previous section.

$$F_c = \gamma * V^2$$
$$F_c = 2.3\,\frac{kg}{m} * b * \left(3.3\frac{m}{s}\right)^2$$
$$F_c = 7.59\; b\; N$$

The manufacturer lists the maximum allowable belt tension as $15.8\frac{N}{mm_{width}}$ [31]. Therefore, the maximum allowable force, $(F_1)_a$, for a belt of unknown width, b, can be found by multiplying the maximum tension by the unknown belt width.

$$(F_1)_a = b * F_a$$
$$(F_1)_a = 15.8\; b\; \frac{N}{mm_{width}} \equiv 15800\; b\; \frac{N}{m_{width}}$$

The force on the slack side belt was solved since the maximum force on the tight side, $(F_1)_a$, is now known. For more information on tight vs. slack side belts, see Appendix A.

$$(F_1)_a - F_2 = \frac{T}{r}$$
$$F_2 = (F_1)_a - \frac{T}{r}$$
$$F_2 = 15800\; b\; \frac{N}{m_{width}} - \frac{184.3\; N\; m}{0.076\; m}$$
$$F_2 = 15800\; b\; \frac{N}{m_{width}} - 2424\; N$$

The minimum belt width can now be found using the Euler-Eytelwein Formula, subtracting centrifugal forces, and solving for b. The coefficient of friction, μ, is listed as 0.22 from the manufacturer's data sheet for contact with a steel pulley [31]. The angle of wrap, θ, is 180° or π rad for two identically sized pulleys.

$$e^{(\mu\theta)} = \frac{(F_1)_a - F_c}{F_2 - F_c}$$

$$e^{(0.22*\pi)} = \frac{15800\ b\ \frac{N}{m_{width}} - 7.59\ b\ N}{15800\ b\ \frac{N}{m_{width}} - 2424\ N - 7.59\ b\ N}$$

$$1.996 = \frac{b}{b - 0.1535}$$

$$b = 0.3144\ m \equiv 12.38"$$

Thus, any belt wider than 12.38” is able to withstand the applied load. We should note that while this calculation found the smallest possible belt width, that was at the maximum permitted load, ignoring belt stretching. For belt longevity, it is best not to load belts to this value. Otherwise, degradation and delamination of the belt splice will occur [38].

Calculating Required Belt Tension

A belt width of 18” (0.457m) was selected to reduce wear and allow the split-belt treadmill to be disassembled into two single-belt treadmills if needed. Next, the load on the tight side, slack side, and initial preload was determined. We will need to use two equations to solve since F_1 and F_2 are both unknown. First, we need to sum the moments around the center of the pulley using Newton’s Second Law, then plug in known values into the Euler-Eytelwein Formula, and finally combine equations to solve for the unknown tensions.

$$F_c = \gamma * V^2$$

$$F_c = 2.3\ \frac{kg}{m} * 0.457\ m * \left(3.2 \frac{m}{s}\right)^2$$

$$F_c = 11.45\ N$$

$$F_1 - F_2 = \frac{184.2\ N\ m}{0.076\ m}$$

$$F_1 - F_2 = 2424\ N$$

$$e^{(\mu\theta)} = \frac{F_1 - F_c}{F_2 - F_c}$$

$$e^{(0.22*\pi)} = \frac{F_1 - 11.45\ N}{F_2 - 11.45\ N}$$

$$1.996 = \frac{F_1 - 11.45\ N}{F_2 - 11.45\ N}$$

We are left with two unknowns and two equations. Using a simultaneous solver program, we arrive at the loads in the tight and slack side belts.

$$F_1 = 4376\ N$$
$$F_2 = 2193\ N$$

This calculation stipulates the minimum allowable belt tension at impending slip in the slack side belt. Thus any tension less than this value will result in the drum spinning faster than the belt. It does not consider the belt's elongation due to the applied load, which will be addressed in a later section.

The minimum required initial belt tension can be determined when the system is at equilibrium. This will occur when the belts are not moving, and the motor is not applying force. This can be done by taking the average of the two values calculated previously, that is when $\mathrm{F}_1 = \mathrm{F}_2$, in other words, when the tight and slack sides have the same tension.

$$F_i = \frac{F_1 + F_2}{2}$$
$$F_i = \frac{4376\ N + 2193\ N}{2}$$
$$F_i = 3284\ N\ or\ 738\ lbs$$

Catenary Load

On the bottom side of the treadmill, the belt will sag under its own weight. This type of loading is often desirable because it increases the tension on the bottom belt and reduces the initial preload required [38]. The deflected shape of the belt is known as a catenary (Fig. 17). While its actual shape is based on hyperbolic trigonometric functions, a close approximation can be reached with a parabolic function when the sag-to-span ratio is small [45].

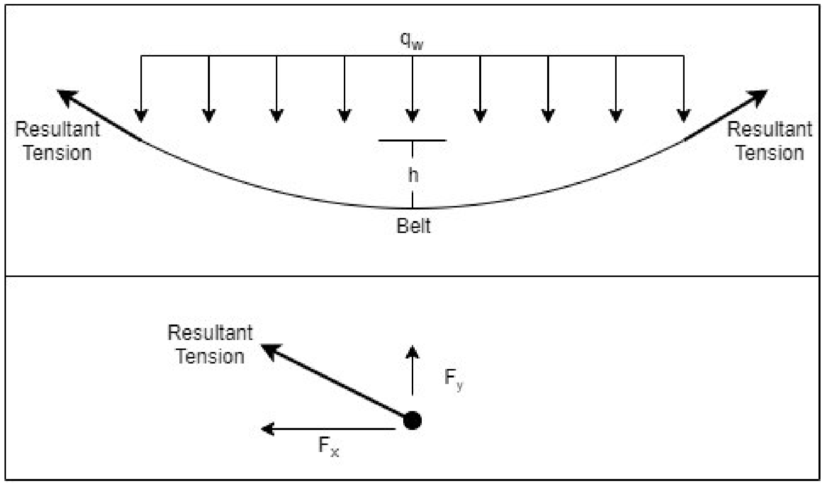

Figure 17. Catenary Cable and Free Body Diagram. The belt, being subject to a distributed gravitational load due to its weight q_w, will sag between its points of contact with the two rollers and reaches a maximum deflection in the middle, h. The free body diagram can be constructed with the resultant tension being broken down into components in the x and y direction.

The manufacturer lists the weight of the belt with units of kg per square meter. This can be converted into units of newtons per meter by multiplying by the acceleration due to gravity and the width of the belt (18” or 0.457 m). The manufacturer-listed weight is $2.3\,\frac{kg}{m^2}$ [31].

$$q = 2.3\ \frac{kg}{m^2} * 0.457\ m * 9.81\frac{m}{s^2}$$
$$q = 10.311\frac{N}{m}$$

Since we already know the minimum horizontal force required to prevent slip, as solved in the belt preload section, we can use the catenary equation, as seen below, to solve for the sag distance [45]. In this equation q_w is the distributed load per unit length, L is the length between supports which was found to be 60.575” (1.54 m), and F_x is the magnitude of the horizontal load.

$$h = \frac{q_w L^2}{8F_x}$$

$$h = \frac{10.311\ \frac{N}{m} * (1.54\ m)^2}{8 * 3284\ N}$$
$$h = 0.0006\ m\ \equiv 0.6\ mm$$

The vertical reaction force F_y (Fig. 17), can be solved by using the equation below. It should be noted that the result is divided by two because each side of the belt shares the same load.

$$F_y = \frac{qL}{2}$$
$$F_y = \frac{10.311 \frac{N}{m} * 1.54\ m}{2}$$
$$F_y = 7.94\ N$$

The magnitude of the resultant load was found by using the Pythagorean theorem and was equal to approximately 3284.01 N, meaning that the tension contribution from the weight of the belt was less than $3 * 10^{-4}$ percent of the total load. Similarly, the angle at the point of contact with the pulley was found to be 0.14° using trigonometric properties. Therefore, the contributions from belt sag are minimal and will not be used in further calculations.

Determining Maximum Belt Elongation Under Load

The belts will stretch when loaded. If we were not to address this elongation, the tension in the slack side would be reduced due to the increased belt length, resulting in insufficient force being applied to the drum and slippage of the belt. Since the belts behave as springs, this can be accounted for by increasing the initial preload. While this is an idealized representation due to the viscoelastic nature of the belt, for the small strains involved and the high strength of the belt material, this approach is sufficient [48].

The belt will be under its highest tension for the longest length when operated in the reverse direction (Fig. 18). Assuming the user is located halfway between the two pulleys, 60.6” between centers, and a 6” diameter pulley, the total length of this section of the belt was found to be 90.9” (2.31 m). The portion of the belt in contact with the driven pulley will not elongate due to friction developed between the two surfaces and thus was not used in this calculation.

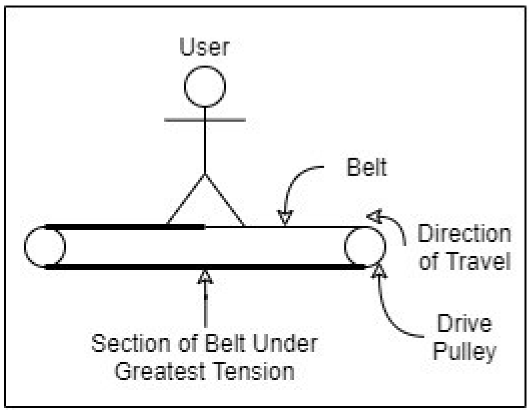

Figure 18. Diagram of Belt Tension in Reverse Operation.

The manufacturer has listed load values required for various percentage elongations (see Appendix J for more information). The load is denoted as having units of Pounds per Inch of Belt Width (PIW). Adding to the complexity is the nonlinear relationship between the load and the amount of elongation (Fig. 19). A best-fit second-order polynomial was found to closely approximate this relationship. Using an automated solver, this equation was found to be $y = 0.0174195x + 0.000515x^2$ for $0 \leq x \leq 90$ PIW, with a correlation coefficient of $R^2 = 0.9984$. Any value greater than 90 PIW will result in failure of the belt material and therefore, should not be used in the calculation. Also, it was assumed that at zero load there would be zero elongation.

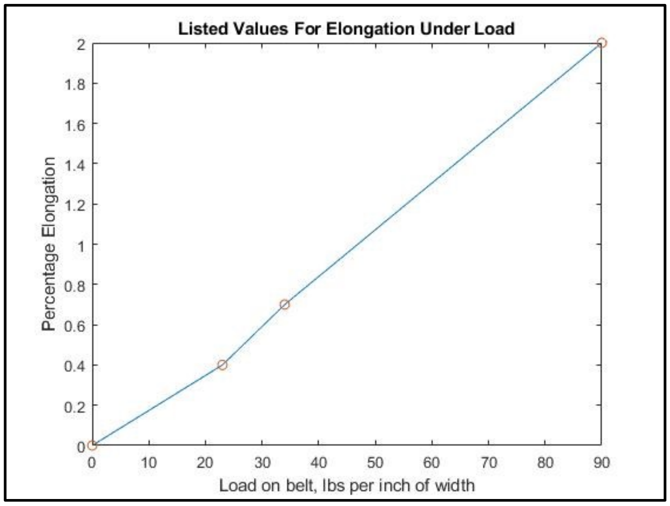

Figure 19. Graph of Belt Elongation Under Load. It can be seen from this plot that the relationship between the loading and elongation is nonlinear.

For the maximum belt tension, which was found to be 4376 N or 983.8 lbs., and an 18" wide belt, the load would be 54 lbs per linear inch of width. Using the best fit curve described previously, this correlates to a 1.16% elongation. Using this value and the formula for percentage change, we can now find the elongation of the belt under load.

$$\%_E = \frac{\Delta L}{L} * 100 \ or \ \Delta L = \frac{L * \%_E}{100}$$

$$\Delta L = \frac{90.9" * 1.16\%_E}{100}$$

$$\Delta L = 1.06"$$

Therefore, the belt will stretch 1.06" when under its highest load giving us a total length of 91.92" for this segment. We can account for this by increasing the preload. Since this tension will be applied over the entire belt, we can find the percentage elongation by dividing the change in length by the length of the entire belt.

$$\%_E = \frac{\Delta L}{L} * 100$$

$$\%_E = \frac{1.06"}{140"} * 100$$
$$\%_E = 0.75$$

The total load this will induce was calculated using the interpolation mentioned previously and was found to be 36.2 PIW or 6.33 N per mm of width.

Determining Total Initial Belt Preload

From a previous section, we found that the minimum load to ensure proper contact with the pulley, when ignoring bet stretch, was $738\ lbs$. This load is applied along the entire width of the belt. Dividing this number by the width of the belt, we get the load per inch of width.

$$PIW = \frac{738\ lbs}{18"}$$
$$PIW = 41\frac{lbs}{in}$$

This can now be added to the value obtained for belt elongation to arrive at the total preload required for the belt.

$$Total\ Preload = 41\frac{lbs}{in} + 36.2\frac{lbs}{in}$$
$$Total\ Perload = 77.2\frac{lbs}{in}$$

With the interpolation mentioned previously, this equated to 1.7%$_E$, which is still within the maximum of 2%. Therefore, the smallest belt that could be used when incorporating belt stretch is 15.5”, which was determined using the calculation procedure laid out in the minimum belt width section.

Notes On Preload and Tension Calculations.

It should be noted that the calculations in the previous sections represent a generous overestimate. Functional testing of the treadmill has shown that even with low levels of tension the belts do not slip. There are several possible reasons for this, but the most likely is that the manufacturer's stated coefficient of friction may be too low. Also, the drums were manufactured by a commercial supplier and came with an enamel paint applied. This could increase the coefficient of friction between the belt and the drum. Additionally, the belt friction formula is known to overestimate the tension required [46]. Therefore, the required tension shown in the previous calculations should be taken with some skepticism.

APPENDIX D:

DETAILED SHAFT DESIGN CALCULATIONS

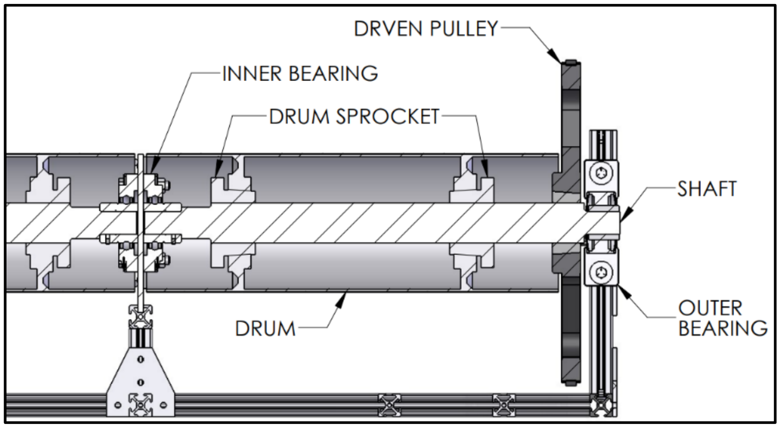

Figure 20. Shaft Component Diagram.
The load from the treadmill belt is transferred from the drum to the shaft via the drum sprockets. The shaft is supported by the inner and outer bearings. Torque is applied via the driven pulley.

<u>Introduction</u>

The components associated with the shafts can be seen in Figure 20. The shafts were designed to withstand the maximum load of all system components. If the shafts fail prematurely, they could become dislodged at speed, presenting a significant risk to those in proximity. Alternatively, the shafts are made of solid steel and add significant weight because four are needed. Therefore, the shafts were designed to be as small as possible while meeting the load requirements.

The loading scenario that was considered for this analysis was that the belts were stretched beyond their breaking point. It is possible that an inexperienced user could apply an excessive initial preload by overtightening the belts, effectively stretching them beyond their rated strength. The belts will not last long at this value, but the shafts must not fail if this happens.

Shaft design is a non-trivial process, often requiring an iterative approach. A rotating shaft under a bending load will experience tension and compression for each shaft revolution. This is known as an alternating state of stress [54]. If the magnitude of the stress is large, this can lead to a phenomenon known as fatigue failure, where the shaft fails suddenly, with little warning [54].

When metals are exposed to alternating stress, they exhibit a material property known as stress endurance limit. This value varies from material to material but exposes a phenomenon known as fatigue limit, where the part will not fail when exposed to a theoretically infinite number of cycles (Fig. 21). While the actual value is based on external properties (part geometry, operating conditions, material strength), it can be calculated using appropriate formulas.

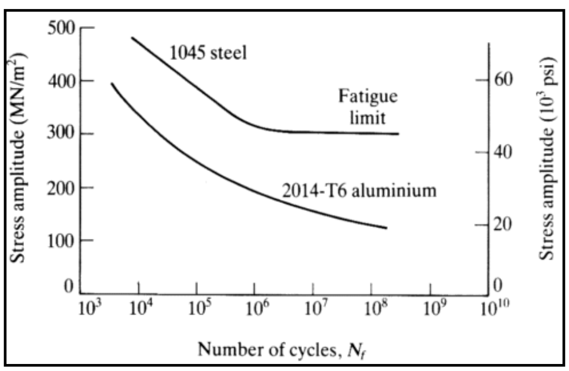

Figure 21. Characteristics of Fatigue Strength for Steel and Aluminum.
It can be seen from this graph that steel exhibits a fatigue limit where an increasing number of cycles do not reduce the fatigue strength. Image source [56].

The procedure for the shaft design was broken up into multiple stages following recommendations from Shigley's Mechanical Engineering Design [54]. First, shear and moment diagrams were constructed. Next, the stress endurance limit for steel was calculated. Finally, the appropriate shaft diameter was found using the Distortion Energy Modified Goodman failure criteria (DE-Goodman).

Loads

The belts selected have a maximum strength of 90 PIW [31]. Multiplying this by the width of the belt (18”), we arrive at a total load of 1620 lbs. This is effectively doubled since both the top and bottom (tight and slack) belts share the load, bringing the total load on the shaft to 3240 lbs. Due to the complexity of generating shear and moment diagrams, a commercially available software package from SkyCiv Engineering was used [57]. A printout of the hand calculations used to verify the numerical solution is included in the GitHub folder for this project (See Appendix J).

Shear and Moment Assumptions and Diagrams

The innermost bearing (Fig. 20) was assumed to act as a pinned support. This is a valid assumption because the set screw in the bearing was tightened to the shaft, restricting axial movement while permitting bending. The outer bearing was modeled as a roller support. The set screws on this bearing were not tightened, allowing for axial movement. The force from the driven pulley was modeled as a point load. The relative contribution to the total force from this component was minor, so this assumption is valid. The load from the treadmill belts is transmitted to the shaft via the drum sprockets. This is modeled as a uniform distributed load with a magnitude of 3240 lbs, divided by the total length of the two sprockets (4in), arriving at a distributed load of 810 lb/in per sprocket. This would represent a worst-case scenario of a fully loaded belt being used at maximum torque. A user on the treadmill causes a tight and slack side belt, and the tension in any singular belt can never be more significant than 1620 lbs. Otherwise, the belt will break. The angle of the resultant force on the shaft from the two belts may change, but the magnitude can never be more significant than double the strength of the belt. The results of this analysis can be seen in Figure 22.

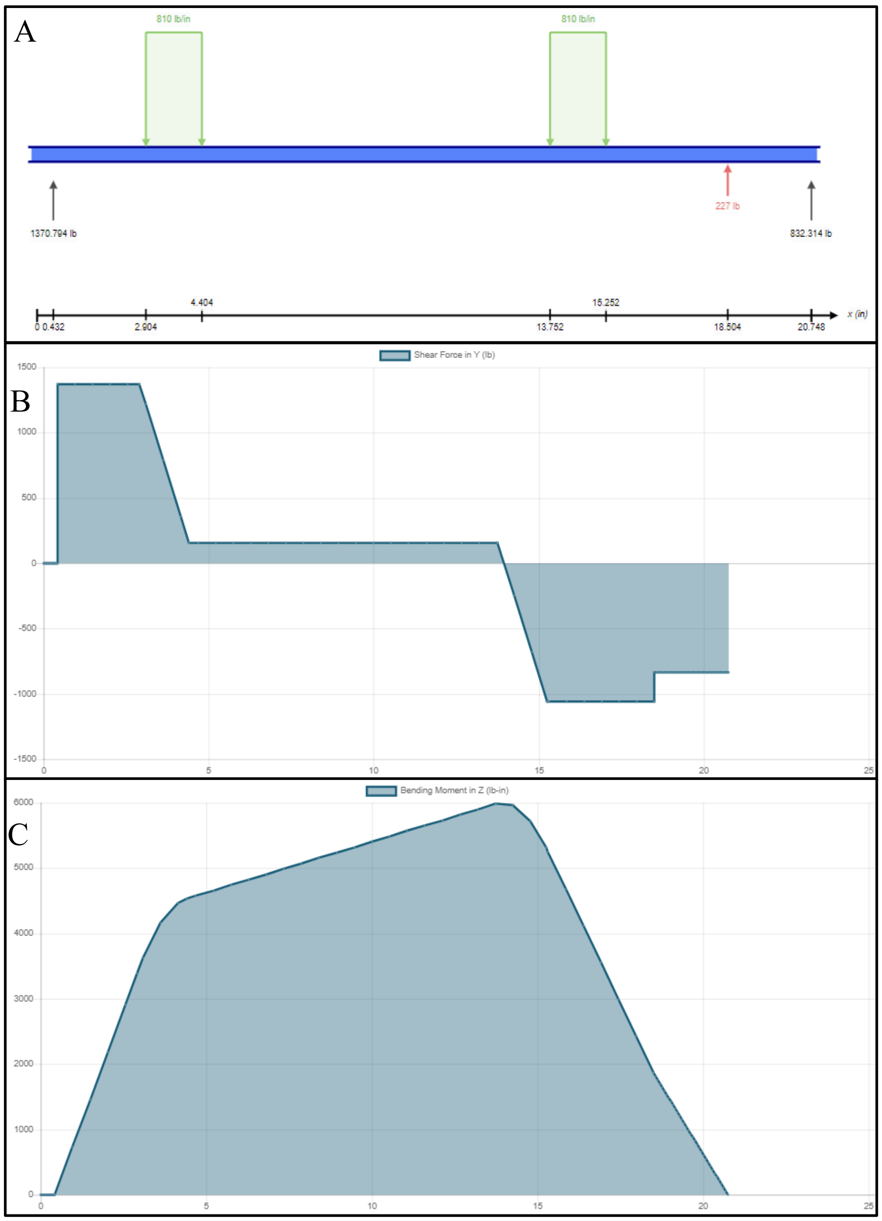

Figure 22. Shear and Moment Diagrams. The free body diagram and reactions are shown in A, the shear force diagram in B, and the bending moment diagram in C. The maximum bending moment of 5990 in.-lbs. was found to occur at 13.75" from the innermost edge of the shaft.

Endurance Limit and Shaft Size

Before an appropriate shaft diameter can be determined, the endurance limit in areas of stress concentrations must be determined. This value effectively reduces the maximum allowable stress for a rotating beam. The formula used to calculate the stress endurance limit is shown below [54].

$$S_e = k_a k_b k_c k_d k_e k_f S'_e$$
$$S_e = \textit{endurance limit at the point of interest}$$
$$k_a = surface\ condition\ modification\ factor$$
$$k_b = size\ modification\ factor$$
$$k_c = load\ modification\ factor$$
$$k_d = temperature\ modification\ factor$$
$$k_e = reliability\ factor$$
$$k_f = miscelanious\ effects\ modification\ factor$$
$$S'_e = rotary\ beam\ test\ specimen\ endurance\ limit$$

Once the endurance limit was determined, the minimum shaft diameter was calculated using the DE-Goodman criteria. While other shaft sizing methods exist, the DE-Goodman was used because it is known to be conservative [54]. The formula for this is as follows.

$$d = \left(\frac{16 * n}{\pi}\left(\frac{A}{S_e} + \frac{B}{S_{ut}}\right)\right)^{\frac{1}{3}}$$
$$A = \sqrt[2]{4\left(K_f M_a\right)^2 + 3\left(K_{fs} T_a\right)^2}$$
$$B = \sqrt[2]{4\left(K_f M_m\right)^2 + 3\left(K_{fs} T_m\right)^2}$$
$$d = diameter\ of\ shaft$$
$$n = desired\ factor\ of\ safety$$
$$S_e = Stress\ Endurance\ Limit$$
$$S_{ut} = Ultimate\ Tensile\ Strength$$
$$K_f = fatigue\ stress\ concentration\ factor\ for\ bending$$
$$K_{fs} = fatigue\ stress\ concentration\ factor\ for\ torsion$$
$$subscripts\ a\ and\ m\ represent\ midrange\ and\ amplitude\ components$$

Values for K_f and K_{fs} were determined with table lookups and a calculated notch sensitivity factor [54]. For a rotating shaft subject to bending and a constant torque, the values for T_a and M_m are zero [54]. Due to the complexity and iterative nature of these calculations, a MATLAB script was created to aid in the design process, which can be found in the GitHub folder associated with this project (See Appendix J). AISI 1045 Cold Rolled Carbon Steel was selected to be the shaft material. Its ultimate tensile strength and yield strength are 84.8 ksi. and 65.3 ksi. respectively [58]. The specific areas of stress concentrations can be seen in Figure 23, and the results of the calculations are shown in Table 5.

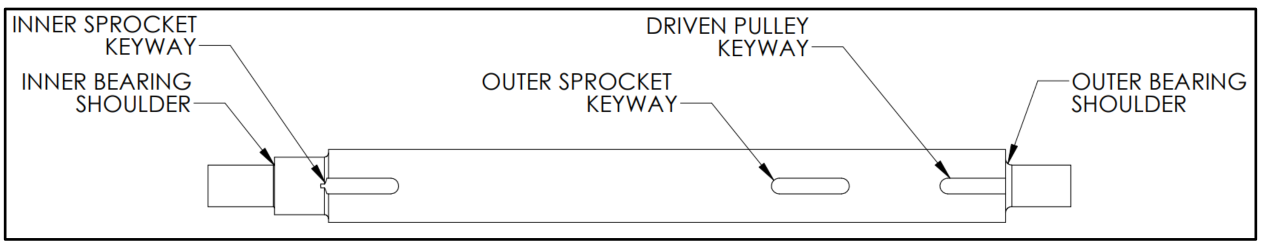

Figure 23. Areas of Interest for Fatigue Life Calculations. Stress concentrations are present in areas of discontinuity along the shaft profile. This can be caused by changing shaft diameter, sharp edges, or notches. These areas need to be examined when sizing the shaft.

Area of Interest	**Type of Stress Concentration**	**Calculated Endurance Limit, S_e $(kpsi)$**	**Bending Moment $(ft\ lb)$**	**Torque $(ft\ lb)$**	**Calculated Minimum Diameter (in)**	**Final Diameter (in)**	**Factor of Safety**
Inner Bearing Shoulder	Shoulder Fillet	25.5	133.5	0	0.941	1	1.2
Inner Sprocket Keyway	Keyway	24.6	347.9	66.5	1.297	1.375	1.4
Outer Sprocket Keyway	Keyway	23.9	495.2	66.5	1.66	1.75	1.2
Driven Pulley Keyway	Keyway	23.9	211.9	133	1.316	1.75	2.4
Outer Bearing Shoulder	Shoulder Fillet	25.5	88.7	0	0.826	1	1.7

Table 5. Summary of Shaft Sizing Results. First, the endurance limit was calculated for the area in question, next values for bending moment, torque, and stress concentrations were entered into the DE-Goodman formula to calculate the minimum size of the shaft, finally the DE-Goodman criteria was used to determine a factor of safety with the selected shaft diameter.

Notes on Shaft Sizing

Cost was a driving factor in the final diameter of the shaft. One-inch bearings were significantly lower in price, thus a lower than ideal, but still acceptable, factor of safety in these areas. It is essential to keep in mind that this loading scenario is an extreme case. The diameter of the shafts was determined based on the breaking strength of the belts, which were in turn sized based on a worst-case scenario of the user standing with both feet on one belt. This results in a compounding factor of safety and oversizing the shafts. During the clinical trial, the treadmill was used for 28 days for approximately five hours each day, and no shaft breakages occurred.

APPENDIX E:

DETAILED BEARING CALCULATIONS

Introduction

Many factors can influence bearing selection, such as shaft speed, total load, and operating conditions. Since bearing manufacturers do not know the specific final operating environment of their products, they typically list the maximum permissible load relative to a known value. This is known as the catalog rating, which is generally rated at 10,000 hours, or 10^6 shaft rotations [59]. The designer can then use this with some specific formulas to select an appropriate bearing.

Assumptions

As a worst-case scenario, it was assumed that the shaft would rotate at the maximum speed the motors would allow, 300 $\frac{Rev}{min}$. As found in the shaft design section, the maximum load was 1062 lbs. and 1370 lbs. for the inner and outer bearings. This is the minimum static load that the bearings need to endure. It was assumed that the majority of the load was occurring in the radial direction, and any axial loads were negligible. Before the final bearing could be selected, the anticipated number of operating hours was determined. As a worst-case scenario, it was assumed that this device would operate continuously for eight hours a day, five days a week for 24 weeks. This is equal to 960 total hours of use.

Calculations and Bearing Selection

The following procedure was used to select the bearings, as outlined in the FYH Mounted Bearing Units Catalog [59]. First, speed factors and life factors were determined. Next, an application factor was used to accommodate for vibrations in the system. Finally, the bearing was selected, and the anticipated bearing life was determined. The formulas used are as follows:

$$C_r = P_r \frac{f_h}{f_n}$$
$$P_r = f_w P_c$$
$$f_h = \left(\frac{L_d}{500}\right)^{\frac{1}{3}}$$
$$f_n = (0.03n)^{\frac{-1}{3}}$$
$$C_r = catalog\ load\ rating$$
$$P_r = corrected\ load$$
$$f_h = life\ factor$$
$$f_n = speed\ factor$$
$$f_w = application\ factor$$
$$L_d = desired\ bearing\ life, hours$$
$$n = desired\ RPM$$

The catalog states that for a toothed belt drive in an operating environment exposed to light impact f_w = 1.1. Carrying out the mathematics, we arrived at the following:

$$P_r = 1.1 * 1062\ lbs. = 1162\ lbs.$$
$$f_h = \left(\frac{960}{500}\right)^{\frac{1}{3}} = 1.24$$
$$f_n = (0.03 * 300\ )^{\frac{-1}{3}} = 0.48$$
$$C_r = 1162 \frac{1.24}{0.48} = 3020\ lbs$$

Therefore, the outer bearing should have a minimum catalog rating of 3020 lbs. Applying the same process to the inner bearing, which must withstand a static load of 1370 lbs., we arrived at a catalog rating of 3896 lbs. After some searching and cost/value analysis, the final bearings were selected, which have the properties listed in Table 6.

Bearing Location	**Type**	**Manufacturer**	**Rated Dynamic Load, (lbs.)**	**Rated Static Load, (lbs.)**
Outer Shaft	Pillow Block	FYH	3,150	1,760
Inner Shaft	4 Bolt Flange	NTN	4,400	2,540

Table 6. Published Data for Selected Bearings. Data sources [59, 60]

Notes on Bearing Selection

Choosing suitable bearings proved to be a challenging obstacle for this project. Typical treadmills or conveyor systems only have a single belt. If that were the case, two pillow block units could be used. Since the design required a tandem belt with a minimal gap between the belts, conventional methods could not be used. The final design features a recessed bearing (Fig. 24), where the inner bearing is hidden behind the drum's outer flange. This not only necessitated a small bearing but one that could withstand a relatively high load. Eventually, a heavy-duty NTN model was selected due to its superior load characteristics and small footprint. With the data in Table 6, the final anticipated life of both bearing units was found to be 1450 hours for the outer unit and 1840 hours for the inner unit. It should be noted that these values are for continuous operation at maximum speed and maximum load. It is not anticipated that while the treadmill is in use, it will operate at max speed continuously, but rather that it will see intermittent periods of high-intensity use. Also, the loads used are for the breaking strength of the belts, which is not indicative of regular operation. Thus, the bearings should last far longer than the computed number of hours.

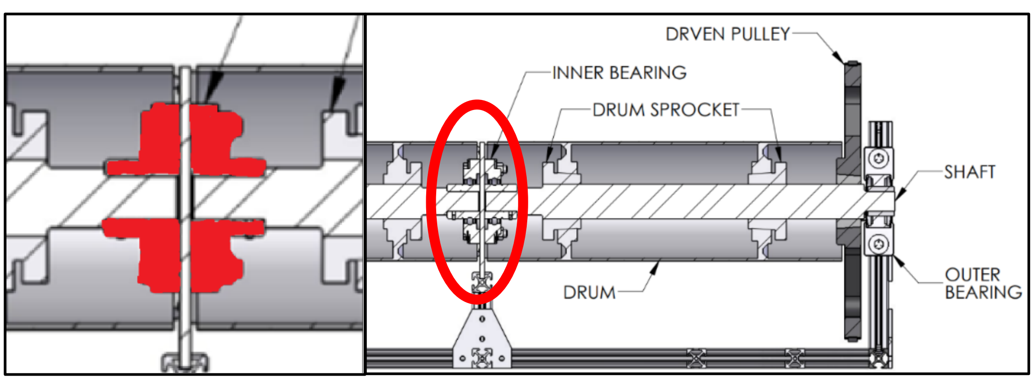

Figure 24. Cross Section of Shaft Showing Recessed Bearing.

APPENDIX F:

DETAILED FRAME ANALYSIS

Introduction

The frame (Fig. 25A) needed to be light and strong to meet the project portability requirements. The majority of the frame components were constructed from lightweight aluminum, with an industry-standard T-Slot profile (Fig. 25C). To further reduce weight and overall project cost, 2-inch sections were only used in areas where stress was a significant concern, with 1-inch sections being used for the remainder of the frame. A specific area of interest was the two horizontal members between the outer bearings (Fig. 25B). These members are under significant compressive stresses, so a column buckling study was performed.

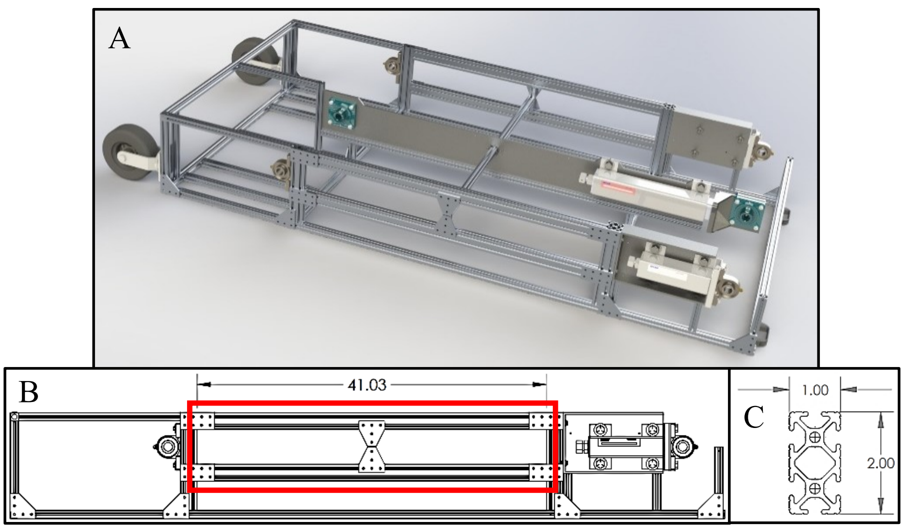

Figure 25. Pictures of the Frame. Image A**.** 3-D rendering of the final frame design showing all components. Image B. Side view with the area in question shown by the red box. Image C. Cross section of 2” x 1” T-Slot.

Background

When subject to a bending load, a traditional beam will deform and give a visual indicator of impending failure, while column buckling failure can be sudden, unexpected, and without warning [54]. It is therefore dangerous, and a critical design analysis is required for this project's safety. The load where buckling becomes a concern is known as the critical load, where any eccentricity or increased force will result in the column becoming unstable [54]. The formula used to calculate the critical load for a long column is known as the Euler Column Formula, which has the following equation [61].

$$\frac{P_{cr}}{A} = \frac{C\pi^2 E}{\left(\frac{l}{k}\right)^2}$$

$$P_{cr} = \text{critical load}$$
$$A = \text{cross sectional area of the column}$$
$$C = \text{end condition constant}$$
$$E = \text{modulus of elasticity}$$
$$l = \text{length of the column}$$
$$k = \text{radius of gyration of column}$$

The slenderness ratio, $\left(\frac{l}{k}\right)$, determines if the column behaves as long, intermediate, or short as defined using the criteria in Table 7.

Beam Type	Criteria	Critical Unit Load
Long	$\left(\frac{l}{k}\right)_{act} > \left(\frac{l}{k}\right)_1$	$\frac{P_{cr}}{A} = \frac{C\pi^2 E}{\left(\frac{l}{k}\right)^2}$
Intermediate	$\left(\frac{l}{k}\right)_1 \geq \left(\frac{l}{k}\right)_{act} \geq \left(\frac{l}{k}\right)_2$	$\frac{P_{cr}}{A} = S_y - \left(\frac{S_y}{2\pi}\frac{l}{k}\right)^2 \frac{1}{CE}$
Short	$\left(\frac{l}{k}\right)_{act} < \left(\frac{l}{k}\right)_2$	$\frac{P_{cr}}{A} = S_y$

Table 7. Criteria and Unit Loads for Column Buckling. The two points used in the criteria are defined as $\left(\frac{l}{k}\right)_1 = \sqrt{\frac{2\pi^2 CE}{S_y}}$ and $\left(\frac{l}{k}\right)_2 = 0.282\sqrt{\frac{AE}{P}}$. In the above equations $\left(\frac{l}{k}\right)_{act}$ is the actual slenderness ratio of the column and S_y is the yield strength of the column material.

<u>Assumptions</u>

It was assumed there was no eccentric loading and the load occurred purely inline and parallel to the centerline of the member. This assumption was made because the bearings are secured to the center slot of the profile, and calculations showed that shaft deflection would be minimal. It was also assumed that the material was free of defects and had homogeneous material properties. The end conditions were assumed to be fixed-fixed, that is the column is not allowed to twist at the connection to the load. Therefore, C=1.2 in the equations listed in Table 7. Finally, Shigley's Mechanical Engineering Design recommends that these equations only be used when a liberal factor of safety is applied [54], so the load will be multiplied by a safety factor of four.

<u>Calculations for Outer Members</u>

The properties of the outer column can be seen in Table 8. The first step was to calculate the radius of gyration of the column.

Material Properties	Material	Aluminum
	Grade	6105-T5
	Modulus of Elasticity, E, [62]	10.2 x 10^6 PSI
	Yield Strength, S_y, [62]	35,000 PSI
Geometric Properties	Cross-Sectional Area, A, [63]	0.7874 in^2
	Minimum Area Moment of Inertia, I, [63]	0.0833 in^4
	Length of Column, l	41.03 in

Table 8. Summary of Properties for T-Slot Sections. The cross-sectional area and area moments of inertia was found using data provided by the manufacturer.

$$k = \sqrt{\frac{I}{A}}$$

$$k = \sqrt{\frac{0.0833}{0.7874}} = 0.3253\ in$$

Next, the slenderness ratio of the part was determined, and it was classified per the criteria in Table 7.

$$\left(\frac{l}{k}\right)_{act} = \frac{41.03}{0.3253} = 126.1$$

$$\left(\frac{l}{k}\right)_1 = \sqrt{\frac{2\pi^2 CE}{S_y}} = \sqrt{\frac{2\pi^2(1.2)(10.2 *\ 10^6)}{35{,}000}} = 83.08$$

Since $\left(\frac{l}{k}\right)_{act} > \left(\frac{l}{k}\right)_1$ the beam can be classified as long, and the critical buckling load can be determined.

$$P_{cr} = \frac{AC\pi^2 E}{\left(\frac{l}{k}\right)^2} = \frac{(0.7874)(1.2)\pi^2(10.2 *\ 10^6)}{\left(\frac{41.03}{126.1}\right)^2} = 5982\ lbs.$$

Therefore, any load greater than 5982 lbs. would be likely to initiate failure by buckling. Next, the actual load was computed by taking the maximum load at the breaking strength of the belts, as computed in a previous section (1062 lbs.), multiplying by a safety factor, and dividing by two since the load is split between the upper and lower outer supports.

$$P_{act} = \frac{1062 * 4}{2} = 2124\ lbs.$$

Since $P_{act} \ll P_{cr}$ the outer support members are unlikely to fail by buckling.

<u>Calculations for Inner Member</u>

The layout for the inner member can be seen in Figure 26. Buckling was a significant concern in this area because the loads from the inner bearings are large, the load can be eccentric, and there are shafts on either side doubling the maximum load.

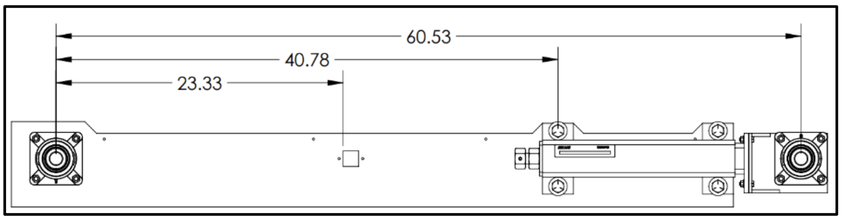

Figure 26. Layout of the Inner Member. The take-up assembly, shown on the right, connects the rear bearings to the inner member.

The front edge of this member is secured by a vertical T-Slot (Fig. 27). Buckling calculations were initially performed with a total column length of 60.53”. It was discovered that this frame section would likely fail unless modifications were made.

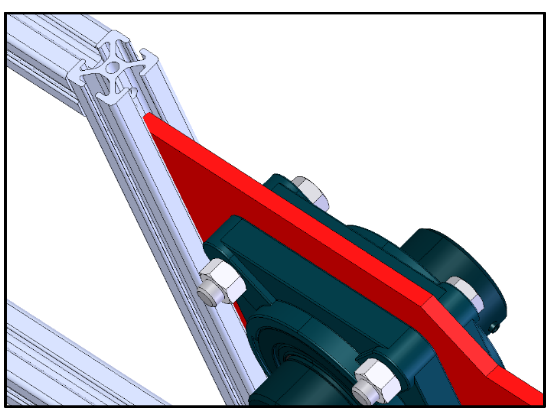

Figure 27. Inner Member Front Connection. The inner member, shown in red for clarity, is restrained by a vertical T-Slot.

To resolve this issue, a horizontal beam was added to minimize deflection in this area, effectively linking the middle and outer sections, as shown in Figure 28L. As an additional safety measure, the center section was fixed in place on the top edge by brackets and the bottom edges by T-Slot, as seen in Figure 28R. This prevents translational movement, ensuring that failure by bucking is not possible.

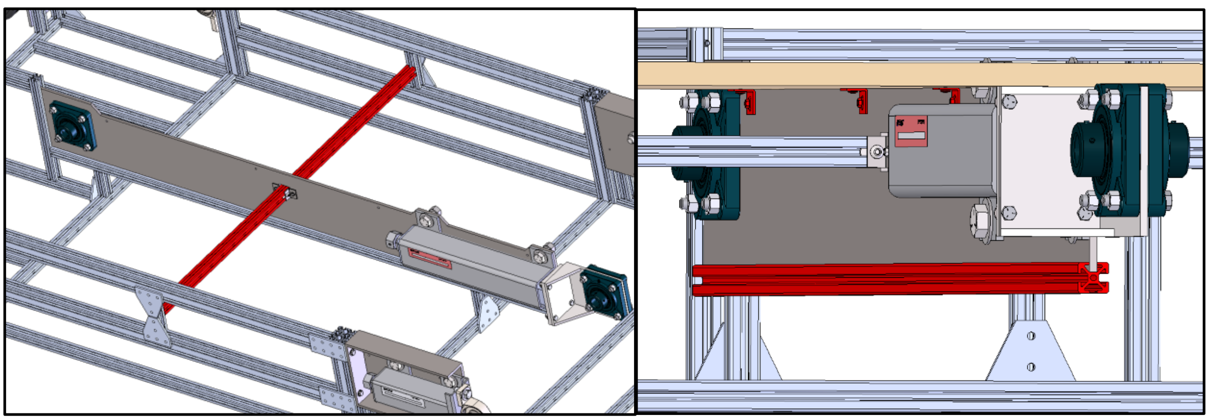

Figure 28. Center Section Reinforcements. Left. Center Beam Link. In order to prevent failure by buckling a horizontal member was added, shown in red for clarity. Right. Supports for Inner Member. The center column was prohibited from lateral movement along its entire length by brackets on the top, and a T-Slot on the bottom, both shown in red for clarity.

<u>Adjusting Belt Tension</u>

Proper belt tension is a critical step in the setup of a treadmill or other conveyor belt-driven devices. If an incorrect amount of tension is applied, either too much or too little, excessive wear and inconsistent performance will result [38]. Too little tension will result in the belts slipping and being unable to drive a load. Too much tension causes excessive wear on the bearings and shafts. The proper amount of tension is the lowest amount that will not cause the belts to slip [38].

Adjustable belt tension is also essential because it directly affects tracking performance. Flat belts have a natural tendency to track towards the side with the lowest tension [41]. If one edge of the belt has more tension than the other, the belt will naturally steer towards that side, which can result in excessive edge wear and loss of contact with the pulley [41].

An early prototype had three adjustment points located at the middle and outer edges of the treadmill (Fig. 29). The central unit is connected to the left and right shafts, while the outer units are only connected to a single shaft, the left or right. This allows for precise tension adjustments on each belt's inner and outer edges.

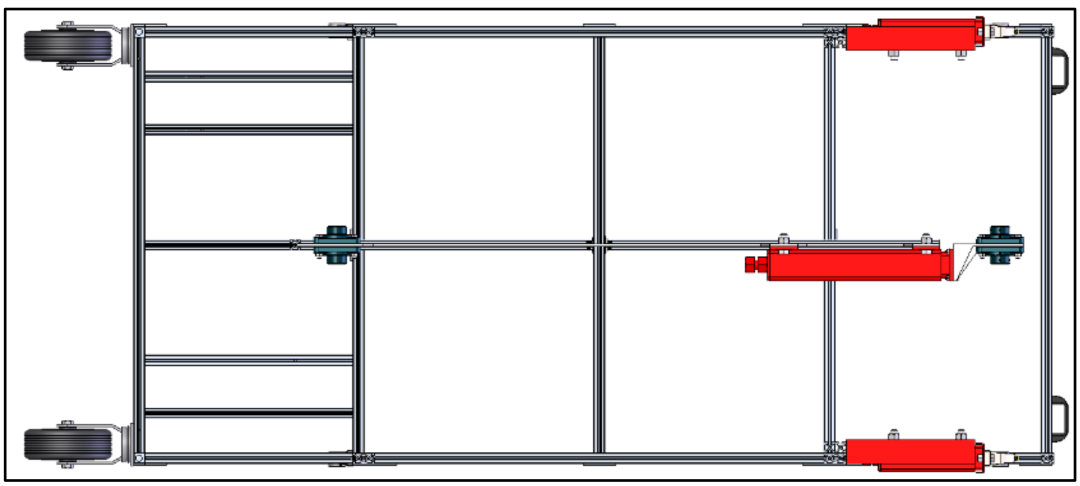

Figure 29. Belt Tension Adjustment Locations. The belt tensioners, shown in red, allow for independent tension and tracking adjustments.

This setup proved to be a problem because the middle adjustment would simultaneously adjust tension for both the left and right belts at the inner edge. If the belts were the exact same length, this would have been adequate but unfortunately, due to manufacturing tolerances or improper storage, the belts were not the same length. This became evident when only one of the belts could be made to track reliably, and we discovered that the right belt was nearly one inch longer than the left. To counteract this, an additional point of adjustment was added to the inner bearing of the right belt (Fig. 30), allowing the right bearing to be slid forward by tightening the set screws on the bearing. This allowed for independent tension adjustments at the inner edge and eliminated most tracking issues.

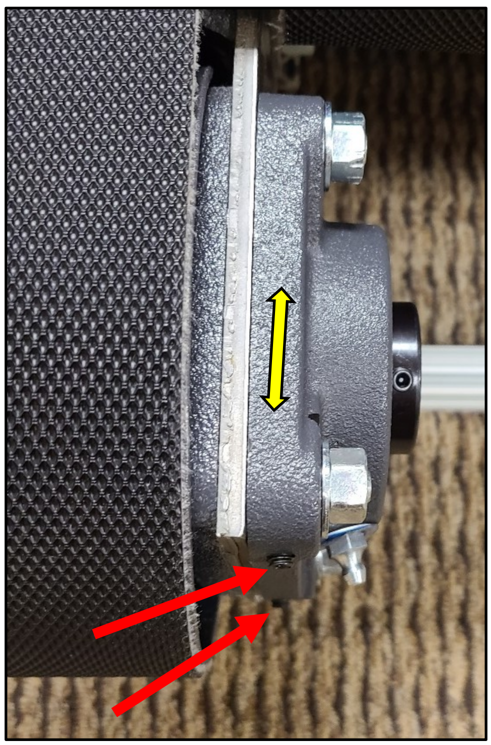

Figure 30. Additional Center Tension Adjustment. The set screws, shown by the red arrows, contact the bolts attaching the bearing to the take-up mechanism. They can be tightened or loosened to move the right bearing block forward or backward relitive to the left shaft.

Belt Tracking

Obtaining reliable belt tracking was the single most challenging aspect of this project. Since crowned pulleys could not be used, belt guides were needed. There is relatively little literature on the design of these guides, and there were no acceptable commercially available units. Therefore multiple prototypes were required before a successful layout was found.

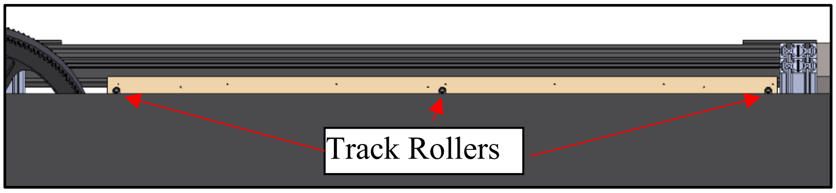

Figure 31. Initial Belt Tracking Method.

The first design used track rollers (Fig. 31), which are ball bearings mounted to a bolt. This design proved unsuccessful because the belt would climb the edge of the roller and lose contact. The rollers were also too small for the mechanical stresses induced by the belts.

The second iteration used two sheets of UHMW to constrain the top and side of the belt (Fig. 32L). This attempt proved unsuccessful because the UHMW did not have enough structural rigidity to prevent the belt from sliding between the two sheets. An aluminum plate was placed on top in an attempt to rectify this issue but it did not resolve the underlying problem.

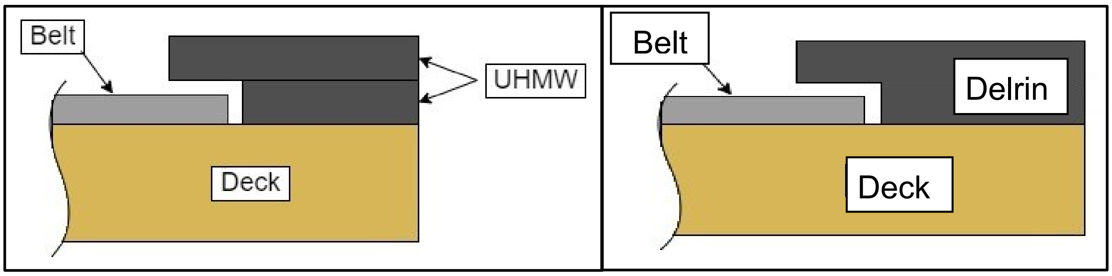

Figure 32. Additional Belt Tracking Methods. Left. Second attempt. Right. Final configuration.

At this point, the project budget had been spent, and no new components could be purchased. Fortunately, a scrap sheet of acetal homopolymer, commonly known by the brand name Delrin, was found in the MSU machine shop. The piece had a sufficient thickness to make the top edge guides out of one component, and a slot was milled for the belt to ride in (Fig. 32R).

Since corrections to belt tracking need to happen before the belt contacts the drum, and the treadmill belt can operate in two directions (forward or reverse), guides were also needed on the lower belt. This was accomplished by milling a slot equal to the thickness of the belt into a 2” block of HDPE, which was then bolted to the side of the frame (Fig. 33L).

For the area between the two belts, no guides were installed. This is because the distance between the belts needed to be as small as possible, and the steel plate that resides there proved to be an adequate guide (Fig. 33R).

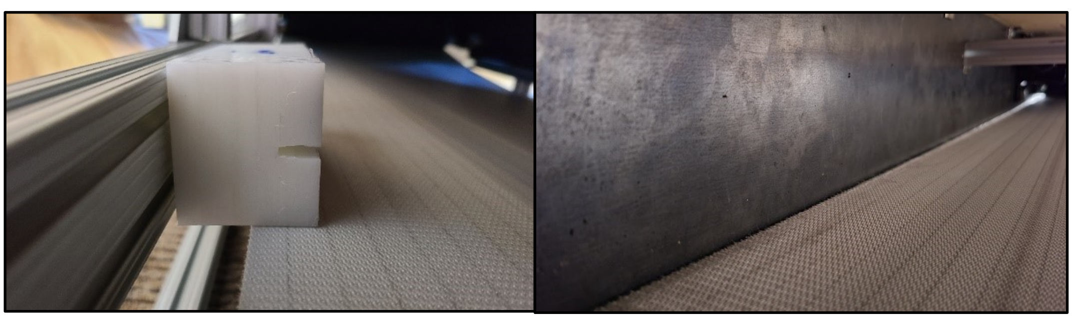

Figure 33. Guides for Lower Belts.Left. Outer guide. Right. Steel plate serving as a guide.

APPENDIX G:

DETAILED HMI DESIGN

Introduction

The motor control box (Fig. 34), also known as the Human Machine Interface (HMI), allows the treadmill to be operated without an external computer by users with little programming experience. The box has been set up to optimize anticipated workflow while minimizing physical size. In the following sections, we will describe the components, anticipated workflow, and wiring diagrams.

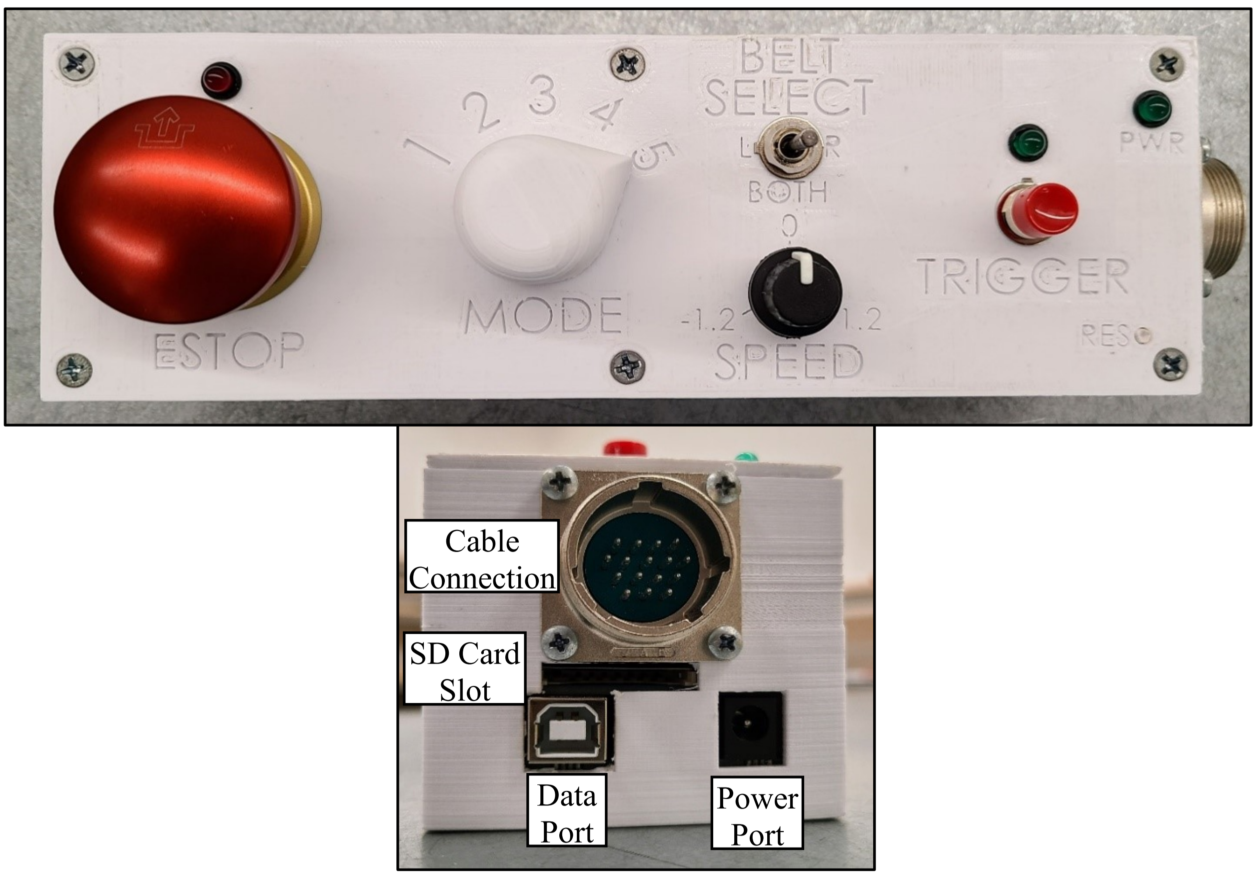

Figure 34. Final Configuration of the Controller Module. Top Image, top-down view showing the buttons, switches, and indicator lights used to control the treadmill. Bottom Image, side view showing the cable, data, and power ports.

Components

- E-Stop Button
    - Allows the operator to shut down the treadmill in case of emergency, self-locking when depressed.
- E-Stop Status LED
    - Red LED that turns on when E-Stop is engaged.
- Mode Select Switch
    - Allows the operator to select from five different belt speed profiles.
- Belt Select Switch
    - Controls whether the perturbation occurs on the left, right, or both belts.
- Belt Speed Potentiometer
    - Sets the desired steady state walking speed in forward or reverse.
- Trigger Button
    - Activates the desired perturbation when depressed.
- Trigger Status LED
    - Green LED that turns on when a perturbation is occurring.
- Power Status LED
    - Green LED that turns on when power is applied to the microcontroller.
- Reset Button
    - Allows the operator to reset the Arduino in case of software errors.
- Cable Connector
    - Connects the controller module to the motors. Allows the box to be disconnected from the rest of the assembly.

- SD Card Slot
    - Can be used to log data or store predefined profiles.
- Data Port
    - Used for data transmission to and from the Arduino, can also be used for power.
- Power Port
    - Secondary power source for the Arduino.

Anticipated Workflow

1. Select the desired perturbation intensity from the mode select switch, 1 is the lowest intensity and 5 is the highest intensity.
2. Slowly ramp up the belt speed to a comfortable steady state walking speed, belt speed can be adjusted in forward or reverse.
3. Use the belt select switch to dictate which belt will run the desired profile. If the switch is set to left or right, the perturbation profile will be performed on the selected belt while the other belt remains at the steady state walking speed. If the switch is in the center position, then both belts will run the perturbation simultaneously.
4. Trigger the perturbation when desired.

Figure 35. Workflow of HMI Buttons.

Wiring Diagram

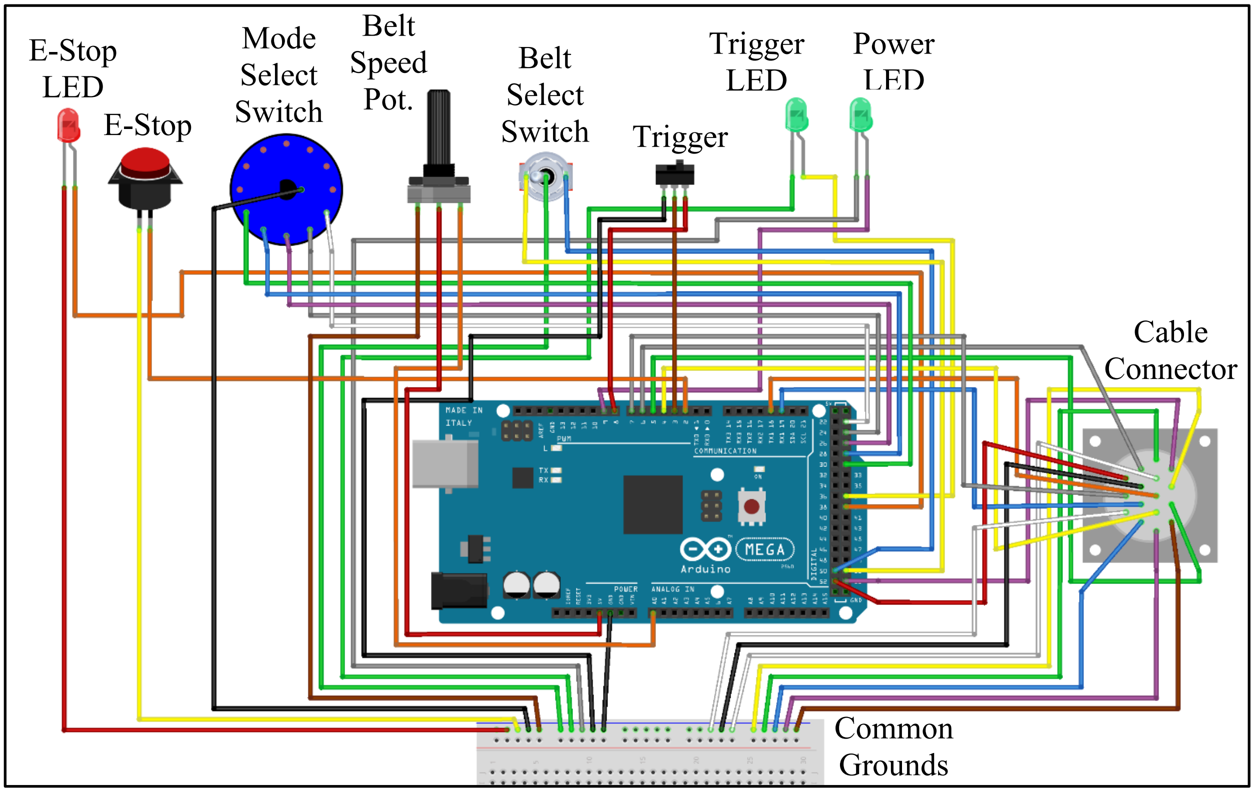

Figure 36. Control Box Wiring Diagram. The wiring diagram shows the Arduino pins the components connect to and the color of the respective wires. There is one omission from this figure, an Adafruit Data Logging Shield is mounted on top of the Arduino. It features a common ground rail that replaces the breadboard in the figure shown, but it was omitted to clearly show the Arduino.

APPENDIX H:

DETAILED SOFTWARE DESIGN

Introduction

The software for the treadmill is broken down into three main components. A motor control program written in C++ runs on the Arduino Mega 2560 within the HMI and is responsible for controlling all functions of the treadmill in real-time. A profile creator, with components written in C++ and Matlab, was used to create new perturbation profiles. Finally, a motor monitor with components written in C++, Matlab, and C# was created to display motor parameters such as speed and torque utilization in real time with a simple graphical interface. The following sections describe these items in more detail, and the code can be found in the GitHub folder for this document (See Appendix J).

Motor Controller

The motor control program serves two primary functions. It continuously monitors the status of the buttons on the HMI and dictates the motor speed. If a button state change is detected, for example the trigger button is pushed, causing the trigger input pin to read high, the software initiates the perturbation. There is also a short debounce interval between button push and code execution to ignore false signals. Motor speed profiles (perturbation profiles) can be defined in two ways. They can be static, where a predefined belt speed profile is stored in memory, or dynamic, where the belt speed profile is calculated on the fly based on HMI button states. The advantage of a dynamically updating profile is its flexibility. It can calculate the profile even if the input states are not fixed. For example, the steady-state walking speed is an input for the perturbation profile calculation routine. This speed can be either positive, negative, or zero. The dynamically updating profile will use this value as an input and recalculate the profile whenever needed, scaling the resulting curves based on the initial speed. The drawback of this approach is that it is memory intensive, and it has been found to not be suitable for profiles lasting longer than two seconds. Although, this could be improved with code optimization and hardware changes. A flowchart for the motor control code can be seen in Figure 37.

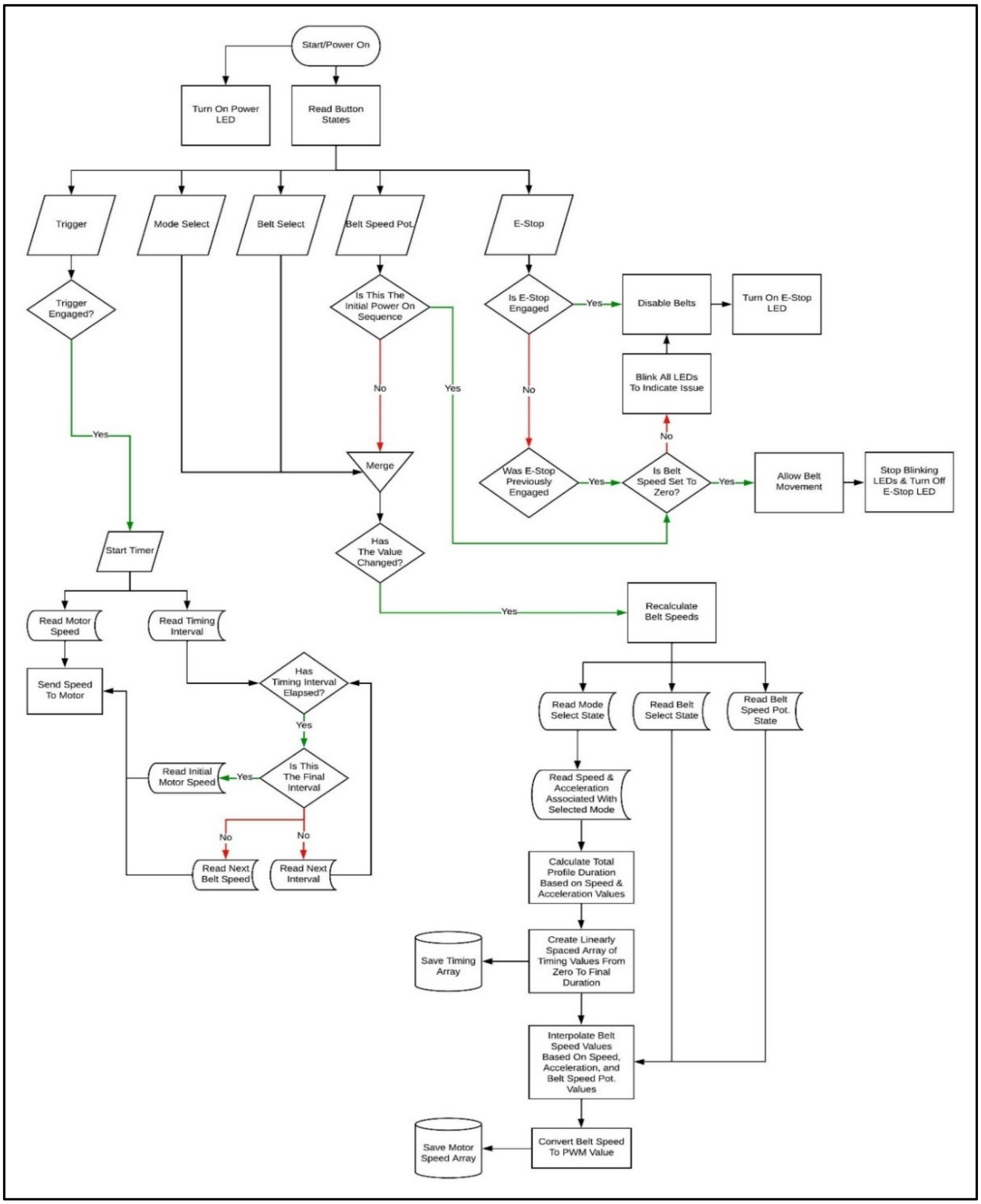

Figure 37. Code Flowchart. A schematic of the software used to control the treadmill.

<u>Creating Perturbation Profiles</u>

The system allows for a great deal of flexibility in how profiles are defined. In its current configuration, constant slope speed versus time plots are generated using a variety of inputs. An example of the perturbation profiles generated can be seen in Figure 38. The program can define these plots in a couple of different ways. Acceleration, acceleration duration, and deceleration values can be specified, or peak speed and duration values, or a combination of the two. In the example shown in Figure 38, a peak speed of 3 m/s was set for mode five. The acceleration and deceleration durations were set at 0.3 and six seconds, respectively. The upper and lower plots show that the peak speed can remain constant even when the belt is set to a non-zero initial speed.

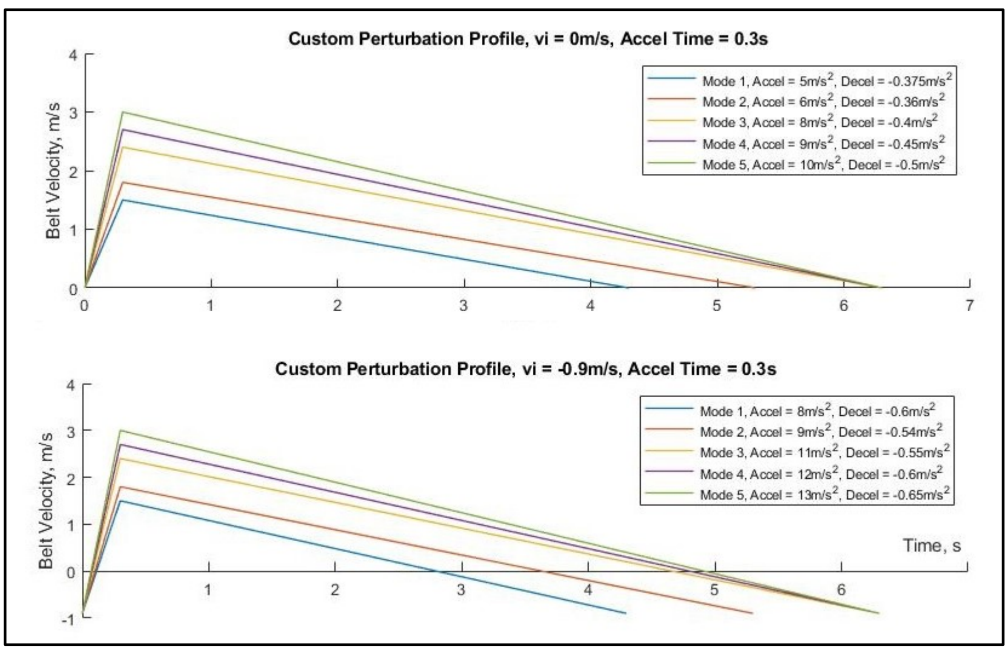

Figure 38. Examples of Perturbation Profiles. Profiles can start with zero initial velocity, as seen in the upper graph, or with a nonzero initial velocity, as seen in the lower graph.

Both types of profiles (static or dynamic) are calculated in the same way. First, the belt speed is converted to motor RPM. Next, the lines between points are interpolated at a rate of 40 samples per second as a compromise between data fidelity and array size. Finally, once the speed and time arrays have been generated, the speed is converted to the data type used by the Arduino Analog Write function. This function, despite its name, generates a digital PWM signal and accepts a byte as input. Since the data must be a byte, an integer ranging from zero to 255, some data fidelity is lost. Each byte increment represents a change of approximately 19 motor RPM. This can be seen by the jagged lines in Figure 39. The user does not feel the sharp edges seen in the profile as there is some elasticity in the system, and the motors have anti-jerk settings enabled.

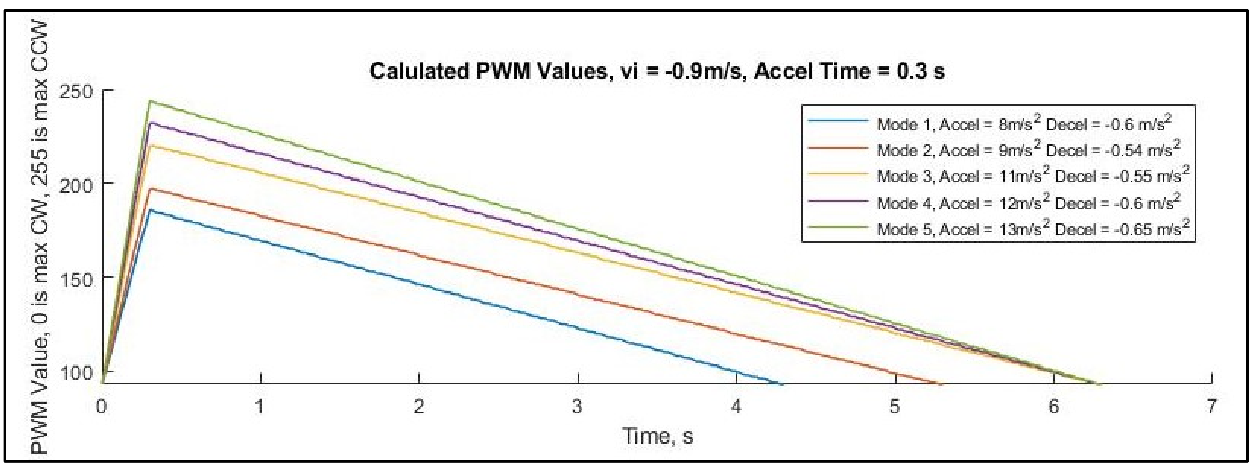

Figure 39. Graph of PWM Signal Sent to Motor. The ridges in the above figure are due to the integer requirement for a byte of data.

Motor Monitor

The motor monitor programs (Fig. 40) were created to display motor status information (belt speed and torque utilization) in real-time. The motors output the actual belt speed as a PWM value. This differs from the commanded speed spent by the Aruiono because the motors have software-defined maximum acceleration values and anti-jerk settings. Torque utilization is also output as a PWM signal. These signals are read by the Arduino using hardware interrupts, and the resulting values are sent to the computer using serial UART communication. There were ultimately two attempts made to display this information on the computer, both suffered lag and latency issues and were not extensively used. The first attempt was a Matlab standalone app. This approach was abandoned when the aforementioned latency issues were discovered. The second attempt was a native Windows application, written in C#, using Microsoft Visual Studio, but the latency issue was still present.

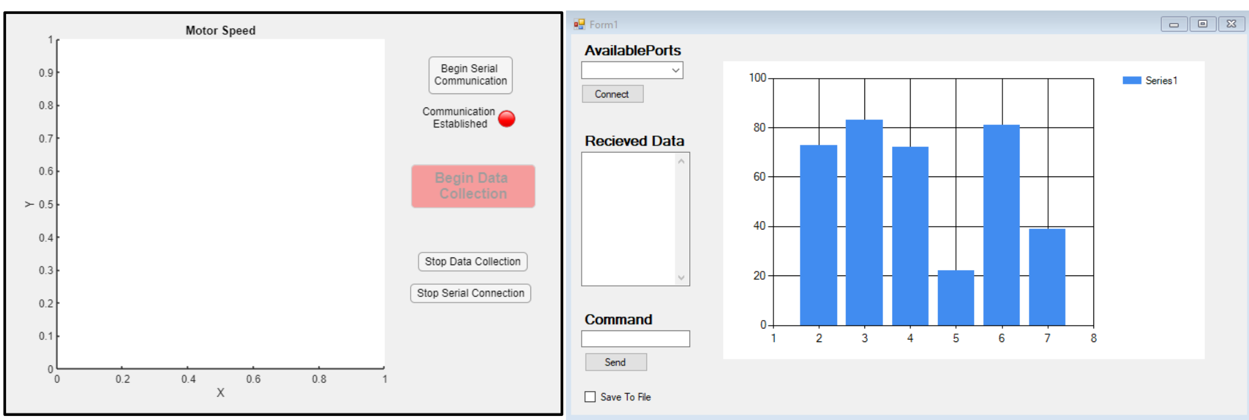

Figure 40. Graphical User Interfaces Used to Display Motor Data. Left. Matlab application created to plot motor speed in real time. Right. Visual Studio application written in C# with the same purpose.

<u>Software Notes</u>

The initial goal was to have all the profiles dynamically update based on the desired steady-state walking speed. After several trials involving long deceleration periods, it was discovered that the Arduino was running out of program storage space and reading from random memory addresses, causing erratic behavior. A MATLAB script was created to predefine the desired profiles to combat this. The script functions the same as the Arduino motor control program but without the benefits of the dynamic profile's flexibility. The output of this program is an array of motor speeds and timing values which are copied into the Arduino's base code.

The software is not limited to purely linear perturbations. Variable slope functions can also be used, such as parabolic, sawtooth, or trigonometric functions (Fig. 41). The custom code allows for a great deal of flexibility in the types of profiles used. It is also important to note that each belt does not have to run the same profile. The software's flexibility allows each belt's speed to be independently controlled.

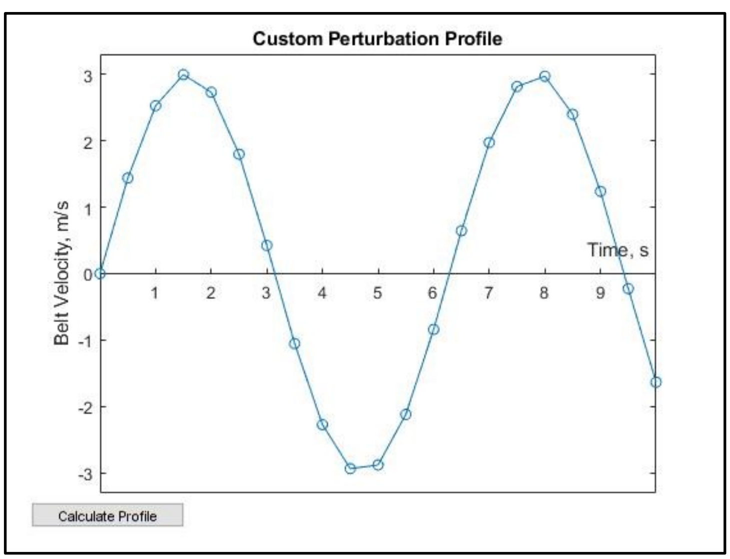

Figure 41. Linear Approximation of Trigonometric Function.

APPENDIX I:

DETAILED DEVICE VALIDATION

Human Analog Test

The goal of this test was to determine if the treadmill would be safe to use under maximum load with human participants. There were three specific questions this test aimed to answer. Are the motors strong enough? Do the belts snap or deform excessively? Is there sufficient tension in the system to prevent slippage of the belts?

The initial system test was performed on a human analog with a reflected load inertia that would match that of a 75-year-old male for 95% of all individuals in this demographic. The mass of the analog was determined by summing the translational and rotational components of the user and solving for an equivalent mass. The values used in the calculations were a user mass of 119 kg [24], a moment of inertia of 12 kg m^2 [49], and a maximum belt speed of 3.3 m/s which is equal to a user rotation rate of 3.4 rad/s.

$$KE_{eq} = KE_{lin} + KE_{rot}$$
$$\frac{1}{2}m_{eq}v^2 = \frac{1}{2}m_u v^2 + \frac{1}{2}I_u w^2$$
$$m_{eq} = \frac{m_u v^2 + I_u w^2}{v^2}$$
$$m_{eq} = \frac{(119\ kg) * (3.3\ {}^{m}/_{s})^2 + (12\ kg\ m^2) * \left(3.4\ {}^{rad}/_{s}\right)^2}{(3.3\ {}^{m}/_{s})^2}$$
$$m_{eq} = 132\ kg \approx 300\ lbs$$

Bags of gravel were used to create the human analog. The gravel was sold in 50 lb. bags therefore, a total of six bags were used. A sheet of expanded polystyrene was placed between the bags and the treadmill belt to prevent excessive wear and increase friction. The setup can be seen in Figure 42.

Figure 42. Human Analog Test. Six bags of gravel were placed on the treadmill to determine if the device would be safe to use under maximum load.

The testing procedure was as follows. Each belt was tested separately. From zero initial velocity, the belts were accelerated at 12 m/s^2 up to 3.3 m/s, then immediately decelerated back to zero at the same rate. The test was performed ten times, and a slow-motion video was recorded to check for slipping between the belt and the drum. After the test, the treadmill was dismantled, and critical loading components were examined. The shafts were checked for hairline fractures, the belts were checked for delamination of the belt splice, and the bearings were checked for low-resistance rotation.

Results of Human Analog Testing

Examining the slow-motion videos revealed no noticeable slippage, proving that there was sufficient tension present in the system. The belt was examined for tears or excessive wear, and none were present. The shaft was placed on a test stand and examined under magnification for hairline fractures using a commercially available die penetrant system. None were found. Motor diagnostic data revealed that the belt reached a peak speed of 3.3 m/s in approximately 0.3

seconds, which is in line with estimates. Therefore, the test was successful, and the system has been validated for a user up to 119 kg.

Human Testing

The human validation of the treadmill was conducted by another student and will be featured in an upcoming Ph.D. dissertation. An undergraduate research assistant, weighing approximately 80kg, stood on the treadmill. They were prevented from falling via a climbing harness attached to an overhead crane. The setup can be seen in Figure 48. XSENS inertial measurement units were used to compare trunk flection angles to previous perturbation studies [20-22]. From zero initial velocity, an acceleration of 12 m/s2 was induced for 0.3 seconds and then decelerated over eight seconds back to zero. Motor diagnostic data were collected during the test to assess torque utilization and system performance.

Figure 43. Setup for the Human Test. An undergraduate research assistant stood on the treadmill and was prevented from falling via a climbing harness attached to an overhead crane.

<u>Results of Human Test</u>

The XSENS data showed that a trunk deflection angle of 26.9° was achieved during the test. Previous studies have reported that the strongest correlation with training-induced improvements to reactive balance occurs at trunk deflection angles above 26.4° [21]. The motor used a maximum of 40% of available torque during the test, as seen by the orange line in Figure 44. After testing, the treadmill was visually examined for excessive wear, and no abnormalities were found. Therefore, the treadmill has been validated and can elicit postural responses similar to slips and trips.

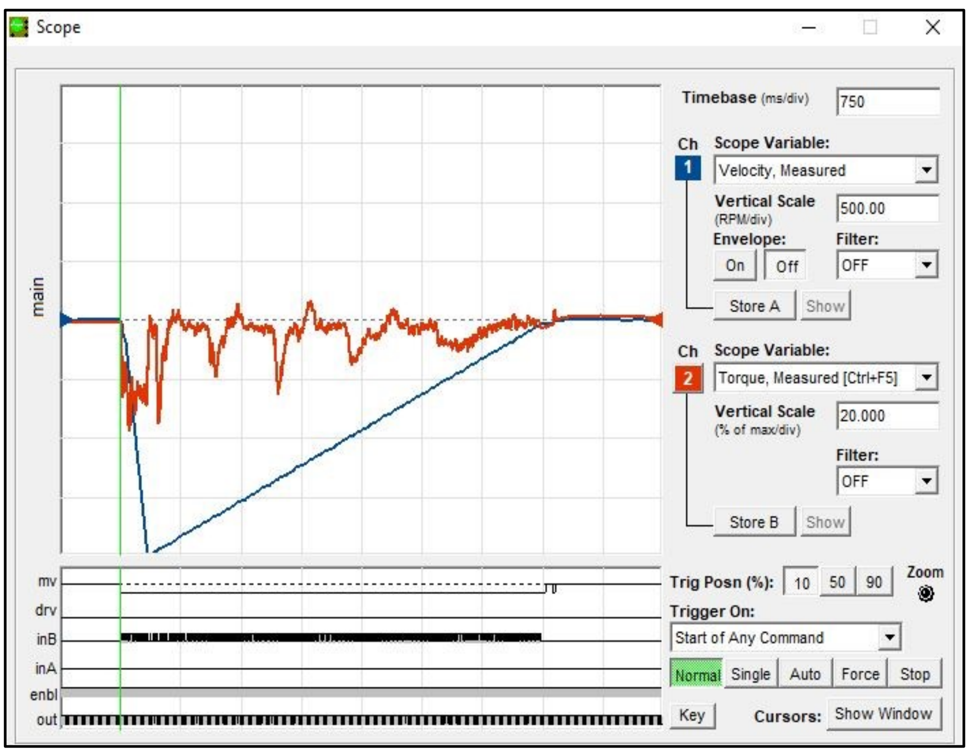

Figure 44. Motor Diagnostic Data Collected During Human Testing. The ticks in the horizontal axis are 750 ms appart. Orange Line. Torque utilization as a percentage of maximum. Individual steps can be seen by spikes in torque utilization. Blue Line. Motor velocity in revolutions per minute.

APPENDIX J:

SUMMARY TABLES, DATASHEETS, & BUDGET

Overview

Several omissions were made in this document to minimize the overall length. Please see the electronic folder associated with this document for more information, such as CAD files, software, and additional recourses. https://github.com/Robert-Knutson/Treadmill

Drivetrain

Component	**Company**	**Model**	**Pitch Circle Diameter** m (in)	**Mass** kg (lb)	**Mass Moment of Inertia** kg cm^2 (lb in^2)	**Max. Angular Acceleration** rad/s	**Max. Velocity** m/s (ft/s)
Driving Timing Belt Pulley	Gates	8MX-25S-12	0.063 (2.506)	0.47 (1.04)	0.033 (0.35)	88	
Driven Timing Belt Pulley	Gates	8MX-140S-12	0.357 (14.036)	6.92 (18.25)	33.04 (470)	15.7	
Drum	PCI	ROL-X46124		10.43 (23)	10.05 (143)	15.7	
Motor	Teknic	CPM-MCVC-N0563P-RLN		11.34 (25)	0.457 (6.5)	88	
Drive Shaft				5.57 (12.28)	0.309 (4.4)	15.7	
Timing Belt	Gates	Gates 8MGT-1440-12		0.46 (1.02)			2.798 (9.18)
Treadmill Belt	MoBelting	2AW5-0BL-SB		3.81 (8.4)			1.494 (4.9)

Bearings

Bearing Location	**Type**	**Manufacturer**	**Rated Dynamic Load, (lbs.)**	**Rated Static Load, (lbs.)**
Outer Shaft	Pillow Block	FYH [59]	3,150	1,760
Inner Shaft	4 Bolt Flange	NTN [60]	4,400	2,540

Frame

Component	**Company**	**Model**	**Material**	**Grade**	**Cross-Sectional Area** in^2	**Minimum Area Moment of Inertia** in^4
1" x 1" T-Slot, [63]	80/20	1010	Aluminum	6105-T5	0.4443	0.0459
1" x 2" T-Slot, [63]	80/20	1020	Aluminum	6105-T5	0.7874	0.0833
1/4" Steel Plate	Online Metals	9610	Steel	A36	1.4915	0.0078

Material Properties

Material	**Grade**	**Modulus of Elasticity** PSI	**Yield Strength** PSI	**Ultimate Tensile Strength** PSI
Aluminum, [62]	6105-T5	10.2×10^6	35,000	
Steel, [64]	ASTM A36	29×10^6	36,300	
Steel, [58]	AISI 1045 CD	29.9×10^6	65,000	84,000

User

Gender	Male
Race	All race and Hispanic-origin groups
Weight	292 lbs (119 kg) [24]
Height	67.4 in (1.71 m) [51]
Mass moment of inertia about frontal axis	23.7 $lb\ ft^2$ (12 $kg\ m^2$) [49, 50]

Data From Human Test

	Trunk Flexion Angle (deg)				
	P1	P2	P3	P4	P5
Max Velocity	1.5 m/s	1.5 m/s	2.6 m/s	3.6 m/s	3.6 m/s
Deel Time	2 s	4 s	6 s	6 s	8 s
T1	17.2	21.5	29.9	29.6	23.1
T2	16.5	18.6	28.8	30.5	26.3
T3	24.6	15.9	28	31.4	28.5
T4	16.8	16.4	23.7	31.6	29.2
T5	22.2	16.3	23	35.5	26.2
T6	14.4	19.6	21.7	28.3	29.8
T7	19.6	18.2	21.5	29	26.5
T8	18.2	16.8	20.2	33.9	23.7
T9	14.2	17.7	21.2	29.8	28.6
T10	15.2	14.3	19	33.2	27.5
Min	14.2	14.3	19	28.3	23.1
Max	24.6	21.5	29.9	35.5	29.8
AVG	18.1	17.6	23.8	31.4	26.9
STDEV	3.2	2.0	3.6	2.2	2.1

The columns denoted by P indicate the perturbation intensity, with five being the highest. The rows denoted by T indicate the specific trial number. The time from perturbation trigger to maximum speed for each trial was 0.3 seconds.

Belt Design Software Datasheet

Industrial Belt Design - Drive Detail Report

Design Flex® Pro by the Gates Corporation

Designed For:

Provided By:
rob knu
Montana State University
anion7.rk@gmail.com
4066720947 Phone

Application: **Design #1**

INPUT

Drive Information			DriveR	DriveN
Speed Ratio:	5.50 Down	RPM:	825.0	150.0 +/-5%
Input Load:	32.9 N-m, Efficiency: 92.00%			
Service Factor:	1.3	Shaft Diameter:	0.625 in	1.75 in
Design Power:	42.77 N-m			
Center Distance:	15 in +/-50%	Bushings Checked:	Any	
Motor Standards:	Electric Motor	Belts Checked:	Poly Chain GT Carbon, Poly Chain ADV, Po	

SELECTED DRIVE

			Belt	DriveR	DriveN
Belt Type:	**Poly Chain GT Carbon - 8MGT**	Part No:	8MGT-1440-12	8MX-25S-12	8MX-140S-12
Speed Ratio:	**5.60 Down**	Product No:	9274-0180	7718-1025	7718-1140
dN RPM:	**147.3**	Pitch Diameter:	--	2.51 in	14.04 in
Rated Load:	**62.32 N-m**	RPM:	114.6	825.0	147.3
ODR:	**1.46**	Rim/Belt Speed:	541 ft/min	528 ft/min	539 ft/min
Belt Pull:	**289 lbf**	Top Width:	--	1.00 in	1.00 in
Center Distance:	14.16 in	**Bushing Part No:**	--	**1108 5/8**	**2012 1 3/4**
Install/Take-Up Range:	13.20 in to 14.20 in	Bushing Product No:	--	7858-0110	7858-2612
		Bore:	--	0.625 in	1.75 in
Noise:	61 dB @ 344 Hz	Bolt Torque	--	55 lbf-inch	280 lbf-inch
		Weight:	0.18 lb	0.70 lb	17 lb
Savings:	The three year savings can be up to 1227 KWh				

TENSION

	New Belt	Used Belt
Static Tension (per rib/strand):	155 to 169 lbf	113 to 127 lbf
Static Belt Pull (total pull):	283 to 309 lbf	206 to 232 lbf
Rib/Strand Deflection Distance:	0.20 in	0.20 in
Rib/Strand Deflection Force:	11 lbf	8.0 to 8.9 lbf
Sonic Tension Meter:	690 to 753 N	502 to 565 N
Belt Frequency:	168 to 176 Hz	143 to 152 Hz

When planning to re-install used belts, measure and record the tension before removing and re-install at the recorded tension.

507C/508C Model STM Settings:
Mass 4.7g/m,Width: 12 mm/#R, Span: 329 mm

NOTES

- Yearly Usage: 5 Hrs / Day, 5 Days / Wk, 50 Wks / Yr

Drive Price	
Belt	$71.29
DriveR	
Pulley	$93.12
Bushing	$18.06
DriveN	
Pulley	$395.78
Bushing	$30.09
Total	**$608.34**

Treadmill Belt Data Sheet

Product Specification Data

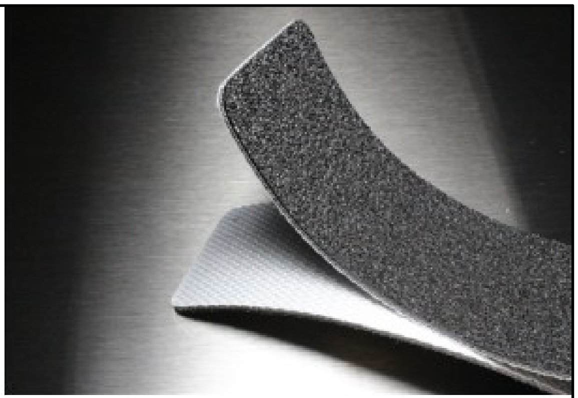

2AW5-0BL-SB
Treadmill

Cover	
Top Color	Black
Thickness	0.03" (0.8mm)
Material	PVC
Pattern	Sand Blast
Durometer	65 A

Carcass	
Plies	2
Fabric	Polyester
Anti-static	Yes
Laterally Rigid	Yes
Pulley Side Material	Polyester Whisper

Weight

0.04 lbs./in.-ft. (2.3 kg/m²)

Maximum Width

84" (2.1m)

Overall Thickness

0.098" (2.5mm)

Minimum Pulley at 70°F	
Min Pulley <180°	1" (25.4mm)
Min Pulley Reverse Bend	2" (50.8mm)

Contact Temperature Range

5°F to 210°F (-15°C to 99°C)

Intermittent Contact Mol Belting

Working Tension	
Minimum	23-34 lbs./in. (4-6 N/mm)
Maximum	90 lbs./in. (15.8 N/mm)

Elongation

0.4% @ 23 lbs./in. (4 N/mm)
0.7% @ 34 lbs./in. (6 N/mm)
2% @ 90 lbs./in. (15.8 N/mm)

Coefficient of Friction	
Mild Steel	0.22
S/S	0.24
UHMW	0.17

Splicing/Lacing Methods	
Splicing	Finger Splice
Lacing #1	
Lacing #2	

Characteristics	
FDA	No
Non-Marking	Yes
Flame Retardant	No
Release Characteristics	Good
Incline Conveying	No
Trough Conveying	No
Swan Neck Conveying	Poor
Metal Detectors (Dependent on Sensitivity)	Contact Mol Belting
Chemical Resistance	See Chart

Accessories	
Edgecap	No
Guide	Yes
Cleats	Yes
Sidewall	Yes
Profile	No

mol belting systems

P 800.729.2358
E sales@molbelting.com
W molbelting.com
Rev. 09/18/2020

Motor Wiring Pin Out

	Motor 1		
5	13	11	2
1	8	3	7

	Motor 2		
4	6	16	9
14	10	15	12

Number in pins above refer to circular connector pin numbers

	Motor 1		
G	G	G	G
53	4	5	18

	Motor 2		
G	G	G	G
52	6	7	19

Number in pins above refer to Arduino pin numbers

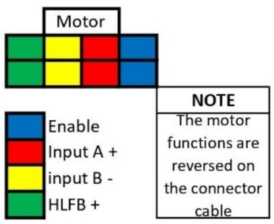

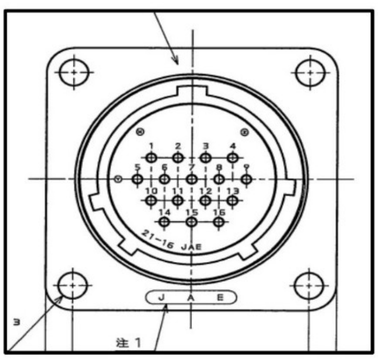

Sub System	Connector Pin	Component Wire Color	Board Wire Color	Funct.	Motor	Arduino Pin
Circular Connector	6	White L	Black	Input A -	1	GND
	10	Grey L	Grey(Gld)	Input A +	2	6
	9	Purple L	Black	HLFB -	1	GND
	12	Blue L	NA	HLFB +	2	19
	4	Brown C	Black	Enable -	1	GND
	14	Red C	NA	Enable +	2	52
	7	Orange L	NA	HLFB +	1	18
	2	Yellow L	Black	HLFB -	1	GND
	5	Green L	Black	Enable -	2	GND
	11	Black C	Black	input B -	2	GND
	16	White C	Black	input B -	2	GND
	15	Grey R	Grey	Input B +	2	7
	1	Purple R	NA	Enable +	1	53
	13	Blue R	Black	Input A -	2	GND
	3	Green R	Yellow	Input B +	1	5
	8	Yellow R	Green	Input A +	1	4
Estop		Orange	Orange	N.O.		2
		Yellow	Black	COM		GND
Rotary Switch		White	White	Pos.1		23
		Grey	Grey	Pos.2		25
		Purple	Purple	Pos.3		27
		Blue	Blue	Pos.4		29
		Green	Green	Pos.5		31
		Black	Black	COM		GND
Trigger Button		Brown	Brown	N.O.		3
		Red	Red	N.C		8
		Black	Black	COM		GND
Potentiometer		Brown	Brown	Gnd		GND
		Red	Orange	Wiper		A0
		Orange	Red	Pos		5v
Belt Switch		Blue	NA	Right		50
		Green	Green	COM		GND
		Yellow	NA	Left		51
Power LED		Purple	Purple	Annode		9
		Grey	Grey	Cathode		GND
Trigger LED		Yellow	NA	Annode		37
		Green	Black	Cathode		GND
Estop LED		Orange	NA	Annode		39
		Red	Black	Cathode		GND

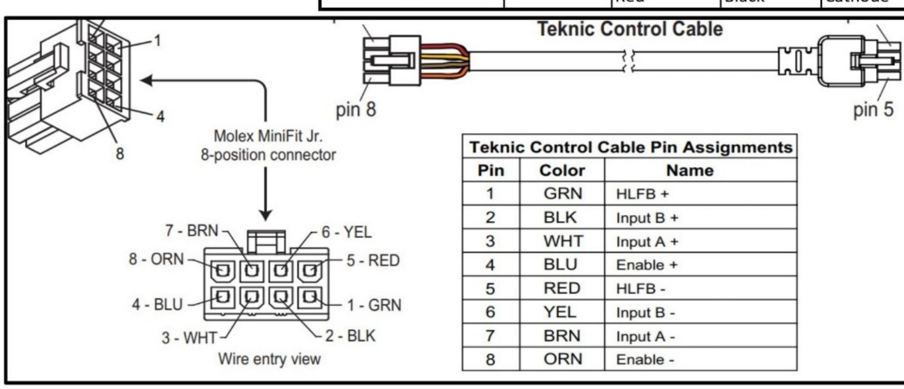

Teknic Control Cable Pin Assignments

Pin	Color	Name
1	GRN	HLFB +
2	BLK	Input B +
3	WHT	Input A +
4	BLU	Enable +
5	RED	HLFB -
6	YEL	Input B -
7	BRN	Input A -
8	ORN	Enable -

Budget

Subsystem	Item	Description	Source	Cost per unit	Qty	Total Cost
Power Transmission	Motor	Electric motor to drive treadmill belt	Teknic	$ 784.00	2	$1,568.00
	Motor Foot	Mounting Bracket for motor	Teknic	$ 14.00	2	$ 28.00
	Driving Pulley	Pulley for motor	RoyalSupply	$ 67.59	2	$ 135.18
	Driving Pulley Bushing	Attaches Driving pulley to Motor Shaft	RoyalSupply	$ 13.35	2	$ 26.70
	Driven Pulley	Pulley for Belt Drive Axle	RoyalSupply	$ 287.33	2	$ 574.66
	Driven Pulley Bushing	Attaches Driven Pulley to Belt Drive Axle	RoyalSupply	$ 21.17	2	$ 42.34
	Drive Belt	Transmits power from motor to Front Treadmill Roller	RoyalSupply	$ 43.87	2	$ 87.74
	Treadmill Belt	Working Surface of Treadmill	WalkingBelts	$ 159.99	2	$ 319.98
	Treadmill Belt Drum	Transmits power from Driven Pulley to Treadmill Belt	Applied	$ 209.15	4	$ 836.60
				Subtotal		$ 3,619.20

Subsystem	Item	Description	Source	Cost per unit	Qty	Total Cost
Frame	Bearings - Center	Mechanical Support for Treadmill Rollers	Grainger	$ 83.58	4	$ 334.32
	Bolts for Front Outer Bearings	1/4-20 1" Long, only sold in 100pk on McMaster, needs T Nut	ACE	$ 0.24	4	$ 0.71
	Washers for Front Outer Bearings	Oversize Washer for 1/4" Bolt, 10pk,	McMaster-Carr	$ 6.06	1	$ 6.06
	Bearing - Outer		McMaster-Carr	$ 39.74	4	$ 158.96
	Bolts for Rear - Outer Bearings	1/2-20 1" Long, 10pk	McMaster-Carr	$ 5.87	1	$ 5.87
	Nuts for Rear - Outer Bearing	1/2-20, Only sold in 100pk on McMaster	ACE	$ 0.11	4	$ 0.44
	Bolts for Center bearings	3/8-16 2" Long, only sold in 50pk on McMaster	ACE	$ 0.32	8	$ 2.56
	Nuts for Center Bearings	3/8-16, Only sold in 100pk on McMaster	ACE	$ 0.09	8	$ 0.72
	Axles	Transmits load from pulley to bearings, 1045 steel CD	Allmetalsinc	$ 61.58	4	$ 246.32
	1" T-Slot Extrusions	Structural Element - 6105 T5 Aluminum - 8 ft sections	McMaster-Carr	$ 23.57	7	$ 164.99
	Double 1" T-Slot Extrusions	Structural Element - 6105 T5 Aluminum - 4 ft sections	McMaster-Carr	$ 20.54	5	$ 102.70
	Track Roller	Guides the belt on the top surface	McMaster-Carr	$ 18.57	14	$ 259.98
	Wood Nuts for Track Roller	8-32 3/4" long, 25pk	McMaster-Carr	$ 10.62	1	$ 10.62
	Outer Belt tensioner	Tensions belt on outer sides	Grainger	$ 206.04	2	$ 412.08
	Bolts for Outer Tensioner	5/8-11 1" Long, 10pk	McMaster-Carr	$ 7.28	1	$ 7.28
	Nuts for Outer Tensioner Bolts	5/8"-11, 25pk	McMaster-Carr	$ 8.51	1	$ 8.51
	Inner Belt Tensioner	Tensions belt in middle	Grainger	$ 293.76	1	$ 293.76
	Center Support Bracket	90 deg T bracket for single rail, Mounting Fasteners included	McMaster-Carr	$ 7.95	8	$ 63.60
	90 deg Deck Support Bracket	Attached deck to Center Middle Frame	McMaster-Carr	$ 0.73	16	$ 11.68
	Screws for Deck Support Bracket	#8 0.75" Fiberboard Screw, Attaches bracket to Deck, only in 100pk on McMaster	McMaster-Carr	$ 9.15	1	$ 9.15
	Bolts for Deck Support Bracket	#8-32 1/2" Long, only in 100pk on McMaster	McMaster-Carr	$ 8.67	1	$ 8.67

Subsystem	Item	Description	Source	Cost per unit	Qty	Total Cost
Frame	Nuts For Deck Support Bracket	#8-32, only sold in 100pk on McMaster	McMaster-Carr	$ 8.36	1	$ 8.36
	T Slot 90 Deg Surface Bracket		McMaster-Carr	$ 7.92	12	$ 95.04
	2 Slot Straight Bracket	Mounting Fasteners included	McMaster-Carr	$ 9.26	8	$ 74.08
	T Slot 3 Way Outside Connector	Connects T Slot meeting at 3 right angles Fasteners Included	McMaster-Carr	$ 10.65	4	$ 42.60
	T Slot Connector Screw	Attaches to threaded hole in center of T Slot	McMaster-Carr	$ 1.79	1	$ 1.76
	Flat Deck Support Bracket	Attaches Deck to Frame	McMaster-Carr	$ 0.92	14	$ 12.88
	Screws for Flat Deck Support Bracket	#5 5/8" Screws for Fiberboard, 100 PK	McMaster-Carr	$ 8.70	1	$ 8.70
	T Slot Nuts	Attaches items to T Slot Channels	McMaster-Carr	$ 0.55	12	$ 6.60
	Cover - Center	Protects Track Rollers from being stepped on	Grainger	$ 3.95	1	$ 3.95
	Screws for Cover Center	8-32 x 1.5" flat head screw, attaches cover to deck, 100pk	McMaster-Carr	$ 8.10	1	$ 8.10
	Nylock Nuts	Low Profile Nylock Nuts 8-32, 100pk	McMaster-Carr	$ 3.23	1	$ 3.23
	Cover - Side	Protects Track Pulleys on Left and Right Sides, Wood, 0.75x0.75x38.5, use same material as deck		$ -	0	$ -
	Fiberboard Screws for Side Cover	#8 1.5" Screws for fiberboard	McMaster-Carr	$ 9.20	1	$ 9.20
	Button Head Screws for Side Cover	1/4-20 5/16" Screws for T Slot, 25 pk	McMaster-Carr	$ 8.84	1	$ 8.84
	T Slot Nuts	1/4-20 Nut for attaching items to T Slots, 25 pk	McMaster-Carr	$ 5.44	2	$ 10.88
	Cover Front - Top	Main Section - Anodized Aluminum 48" x 24"	OnlineMetals	$ 41.23	1	$ 41.23
		Pulley Covers - Anodized Aluminum 24" x 12"	OnlineMetals	$ 13.42	2	$ 26.84
	Cover Center	Attaches to Electrical Enclosure - use leftover from front	OnlineMetals	$ -	0	$ -
	Frame Middle Structural	0.25" Steel A36 HR, 8" x 72"	OnlineMetals	$ 91.27	1	$ 91.27
	Rear Center Take-up Bracket	0.25" Steel A36 HR, 6" x 12" use leftover form middle	OnlineMetals	$ -	0	$ -
	Belt Tensioner Bracket	0.25" Steel A36 HR, 12" x 15"	OnlineMetals	$ 40.45	2	$ 80.90
	Bolts for Belt Tensioner Bracket	1/4-20 0.5" Long, only sold in 100pk on McMaster, needs T Nut	ACE	$ 0.13	4	$ 0.52
	Bolts for Motor Mounts	1/4-20 0.5" Long, only sold in 100pk on McMaster, needs T Nut	ACE	$ 0.21	8	$ 1.68
	Wheels	Rubber wheel barrel wheels, fixed, 6in OD	McMaster-Carr	$ 14.24	2	$ 28.48
	Deck	3/4" MDF, 4' x 8' Sheet	HomeDepot	$ 41.47	1	$ 41.47
	Deck Top Surface	Provides slippery surface, prevents wear to deck	McMaster-Carr	$ 50.76	3	$ 152.28
				Subtotal		**$ 2,804.82**

Electronics	240V 50A Power Cord	Extension Cord for Generator	Amazon	$ 279.99	1	$ 279.99
	Arduino Mega 2560	Microcontroller	ArduinoStore	$ 40.30	1	$ 40.30
	Arduino data logger	SD Card Shied for Arduino	Adafruit	$ 13.95	1	$ 13.95
	SD Card	8 GB, Micro SD but comes with adapter	Adafruit	$ 9.95	1	$ 9.95
	USB Cord	10 ft USB A to B	Teknic	$ 9.00	1	$ 9.00

Subsystem	Item	Description	Source	Cost per unit	Qty	Total Cost
Electronics	Power Adapter	9 V, 1.5 A, 6 ft cord	Amazon	$ 8.99	1	$ 8.99
	E Stop Button	Large button to send stop command to motor	Automation Direct	$ 36.00	1	$ 36.00
	E Stop Button Contacts	(1) N.O./(1) N.C. Position 1	Automation Direct	$ 9.75	1	$ 9.75
		(1) N.O./(1) N.C. Position 2	Automation Direct	$ 9.75	1	$ 9.75
		(1) N.O./(1) N.C. Position 3	Automation Direct	$ 9.75	1	$ 9.75
	Case for Arduino and E Stop	3D Printed, no cost	Self	$ -	0	$ -
	Data Cable to Treadmill	22 GA by 10 ft	Teknic	$ 23.00	2	$ 46.00
	240 V Electrical Plug & Enclosure	Plug that connects motor power cables to generator extension cord	Amazon	$ 33.38	1	$ 33.38
	12 GA Wires for Motor Power	3 Wire TPE Overmold, only ships in 20' increments, 0.435" OD	Automation Direct	$ 17.20	1	$ 17.20
	Strain Relief for Motor Power	3/4" knockout electrical passthrough	Grainger	$ 6.14	2	$ 12.28
	16-pin female headers	Connects to Data Cable	Digikey	$ 6.68	1	$ 6.68
	16-pin male headers	Mounted to Control Box	Digikey	$ 12.87	1	$ 12.87
	5 pos rotary switch SP5T	Mode Switch	Digikey	$ 5.87	1	$ 5.87
	Momentary switch	Trigger Switch	Digikey	$ 3.48	1	$ 3.48
	LED indicator Light - Green	Status indicator light	Digikey	$ 2.09	2	$ 4.18
	LED indicator Light - Red	Status indicator light	Digikey	$ 2.09	1	$ 2.09
	Panel Mount Center Detent Potentiometers	Belt Speed Potentiometer	Mouser	$ 1.19	1	$ 1.19
	Potentiometer Knob - Soft Touch T18 - White	Belt Speed Knob	Mouser	$ 0.50	1	$ 0.50
	Toggle Switches SPDT ON-OFF-ON SLDR	Belt Select Switch	Mouser	$ 3.09	1	$ 3.09
	Switch Hardware DRESS NUT	Cosmetic nut for trigger button	Mouser	$ 1.39	1	$ 1.39
	Jumper Wires	Used to connect components inside Control Box 250pk	Mouser	$ 13.25	1	$ 13.25
	Heat Shrink Tubing	Used to keep electrical components from shorting 100 pk	Mouser	$ 9.95	1	$ 9.95
				Subtotal		**$ 617.35**

Extras	Generator	Auxiliary power, 12000 W Continuous	HomeDepot	$ 1,399	1	$1,399
	Gorilla Wood Glue	Keeps wood nuts from pulling out	HomeDepot	$ 7.99	1	$ 7.99
	Red Loctite	Used to keep bolts tight	HomeDepot	$ 4.99	1	$ 4.99
				Subtotal		**$ 1,411.98**
				Shipping Total		**$ 1,706.99**

Overall Total $ 10,144.65

For more detailed budget information, including manufacturer's part numbers and hyperlinks, see the cloud folder for this project, https://github.com/Robert-Knutson/Treadmill

REFERENCES CITED

1. Rubenstein, L.Z., *Falls in older people: epidemiology, risk factors and strategies for prevention.* Age and Ageing, 2006. **35**(suppl_2): p. ii37-ii41.

2. Moylan, K.C. and E.F.J.T.A.j.o.m. Binder, *Falls in older adults: risk assessment, management and prevention.* 2007. **120**(6): p. 493. e1-493. e6.

3. Sattin, R.W.J.A.r.o.p.h., *Falls among older persons: a public health perspective.* 1992. **13**(1): p. 489-508.

4. Katsoulis, M., et al., *Excess mortality after hip fracture in elderly persons from Europe and the USA: the CHANCES project.* 2017. **281**(3): p. 300-310.

5. Landi, F., et al., *Sarcopenia as a risk factor for falls in elderly individuals: results from the ilSIRENTE study.* 2012. **31**(5): p. 652-658.

6. Sherrington, C., et al., *Effective exercise for the prevention of falls: a systematic review and meta-analysis.* Journal of the American Geriatrics Society, 2008. **56**(12): p. 2234-2243.

7. Pai, Y.-C., et al., *Perturbation training can reduce community-dwelling older adults' annual fall risk: a randomized controlled trial.* Journals of Gerontology Series A: Biomedical Sciences and Medical Sciences, 2014. **69**(12): p. 1586-1594.

8. McCrum, C., et al., *A systematic review of gait perturbation paradigms for improving reactive stepping responses and falls risk among healthy older adults.* European review of aging and physical activity, 2017. **14**(1): p. 1-11.

9. Lurie, J.D., et al., *Pilot comparative effectiveness study of surface perturbation treadmill training to prevent falls in older adults.* BMC geriatrics, 2013. **13**(1): p. 1-8.

10. Lurie, J.D., et al., *Surface perturbation training to prevent falls in older adults: a highly pragmatic, randomized controlled trial.* 2020. **100**(7): p. 1153-1162.

11. Shapiro, A. and I. Melzer, *Balance perturbation system to improve balance compensatory responses during walking in old persons.* Journal of neural engineering, 2010. **7**(1): p. 1-6.

12. *Instrumented Treadmills*. Bertec Co.

13. Chen, C., et al., *Development of a three-degrees-of-freedom moveable platform for providing postural perturbations.* 2009. **223**(1): p. 87-97.

14. U.S. Census Bureau. *American Community Survey 5-year estimates*. 2020; Available from: http://censusreporter.org/profiles/04000US30-montana/.

15. Whitten, J., Oleary B., Tarabochia, D., Graham, D. , *Does Perturbation-Based Balance Training on Commercial Treadmills Improve Balance Recovery in Older Adults?* , in *Gerontological Society of America (GSA) Conference* 2022: Indianapolis, IN, USA.

16. Redfern, M.S., et al., *Biomechanics of slips.* 2001. **44**(13): p. 1138-1166.

17. Allin, L.J., M.A. Nussbaum, and M.L.J.E. Madigan, *Feet kinematics upon slipping discriminate between recoveries and three types of slip-induced falls.* 2018. **61**(6): p. 866-876.

18. Grabiner, M.D., et al., *Kinematics of recovery from a stumble.* 1993. **48**(3): p. M97-M102.

19. König, M., et al., *Retention of improvement in gait stability over 14 weeks due to trip-perturbation training is dependent on perturbation dose.* 2019. **84**: p. 243-246.

20. Wang, Y., et al., *Can treadmill-slip perturbation training reduce immediate risk of over-ground-slip induced fall among community-dwelling older adults?* 2019. **84**: p. 58-66.

21. Aviles, J., et al., *Improvement in trunk kinematics after treadmill-based reactive balance training among older adults is strongly associated with trunk kinematics before training.* 2020. **113**: p. 110112.

22. Feldman, A.G., et al., *Changes in the referent body location and configuration may underlie human gait, as confirmed by findings of multi-muscle activity minimizations and phase resetting.* 2011. **210**(1): p. 91-115.

23. Bieryla, K.A., M.L. Madigan, and M.A. Nussbaum, *Practicing recovery from a simulated trip improves recovery kinematics after an actual trip.* Gait & posture, 2007. **26**(2): p. 208-213.

24. Fryar, C.D., et al., *Anthropometric Reference Data for Children and Adults: United States, 2015-2018.* Vital & Health Statistics, 2021(36): p. 1-44.

25. McCrum, C., et al., *Older adults demonstrate interlimb transfer of reactive gait adaptations to repeated unpredictable gait perturbations.* 2020. **42**(1): p. 39-49.

26. Golyski, P.R., et al., *Onset timing of treadmill belt perturbations influences stability during walking.* 2022. **130**: p. 110800.

27. Sessoms, P.H., et al., *Method for evoking a trip-like response using a treadmill-based perturbation during locomotion.* 2014. **47**(1): p. 277-280.

28. *SIZE OF A PICKUP TRUCK BED*. Available from: https://tailoredtrucks.com/blog/size-of-a-pickup-truck-bed/.

29. HEARST AUTOS RESEARCH. *How Long Is a Long Bed Truck:*. 2020; Available from: https://www.caranddriver.com/research/a32811097/how-long-is-a-long-bed-truck/.

30. Waters, T., V. Putz-Anderson, and A. Garg, *Applications manual for the revised NIOSH lifting equation*. DHHS publication ; no. (NIOSH) 94-110;. 1994.

31. *Product Specification Data Model 2AW5-0BL-SB*. 2020; Available from: https://www.molbelting.com/belts/2AW5-0BL-SB.

32. DuoMaxPower. *13,000 Watt Dual Fuel Portable Generator*. n. d. November 9, 2022]; Available from: https://www.duromaxpower.com/products/duromax-xp13000eh-13000-watt-portable-hybrid-gas-propane-generator.

33. Waehner, P. *What to Look for If You Buy a Treadmill*. 2019; Available from: https://www.verywellfit.com/buying-a-treadmill-1229609#:~:text=Minimum%20Specifications,-Other%20things%20to&text=Belt%20size%3A%20For%20running%2C%20the,54%2Dinch%20belt%20for%20running.

34. Bye, D. *Proper Treadmill Size*. Available from: https://www.livestrong.com/article/286794-proper-treadmill-size/.

35. *Which Size Treadmill Do You Need? Treadmill Belt Size*. Available from: https://homegymresource.com/which-size-treadmill-do-you-need-treadmill-belt-size/.

36. *Treadmill Belts Suppliers*. Thomas.

37. Hamacher, S., *Types of conveyor belts*, in *The Drum Motor*. 2020, Springer. p. 11-27.

38. *Belt Conveyors for Bulk Materials*. 7th ed. 2020: CEMA.

39. Span Tech Conveyors. *Guide to Conveyor Belt Tracking* 2022 2022/04/18/; Available from: https://spantechconveyors.com/2022/04/15/guide-to-conveyor-belt-tracking.

40. Egger, M., K.J.J.M.E. Hoffmann, and Automation, *Tracking of flat belts.* 2012. **2**: p. 27-36.

41. *Fabric Conveyor Belts Engineering Guide*. Habasit AG.

42. Egger, M., K. Hoffmann, and F.-W.T. Wien. *Lateral running of flat belts: The angled conical pulley*. in *Int. Conf. Mechanism and Machine Science*. 2007.

43. Euler, L., *Remarques sur l'effet du frottement dans l'equilibre*. 1769: J Memoires de l'academie des sciences de Berlin. 265-278.

44. Johnson, K.L. and K.L. Johnson, *Contact mechanics*. 1987: Cambridge university press.

45. Meriam, J. and L. Kraige, *Engineering Mechanics: Statics: Statics*. 2011: Wiley Global Education.

46. P.E, B.D., *Variant Friction Coefficients of Lagging and Implications for Conveyor Design.* CEMA Net, 2015.

47. Grashof, F., *Theoretische Maschinenlehre.* L. Voss, Leipzig, Germany, 1890.

48. Kong, L. and R.G.J.P.o.t.I.o.M.E. Parker, Part C: Journal of Mechanical Engineering Science, *Microslip friction in flat belt drives.* 2005. **219**(10): p. 1097-1106.

49. Nigg, B.M. and W. Herzog, *Biomechanics of the musculo-skeletal system*. 2007: Wiley.

50. Santschi, W.R., J. Dubois, and C. Omoto, *Moments of inertia and centers of gravity of the living human body*. 1963, NORTH AMERICAN AVIATION INC LOS ANGELES CA.

51. Ogden, C.L., *Mean body weight, height, and body mass index: United States 1960-2002*. 2004: Department of Health and Human Services, Centers for Disease Control and ….

52. *Design Flex Pro*. Gates Corporation.

53. *Polychain GT Carbon Belt Drive Systems*. 2009, Gates Corporation. p. 46.

54. Nisbett, K. and R. Budynas, *Shigley's Mechanical Engineering Design, 10th Edition*. 2015.

55. *CLEARPATH MOTORS AC INPUT, INTEGRAL HORSEPOWER*. Teknic Inc.

56. *Fatigue Strength*. Available from: https://www.efunda.com/formulae/solid_mechanics/fatigue/fatigue_highcycle.cfm.

57. *Shaft Desiginer*. June 30, 2022]; Available from: https://platform.skyciv.com.

58. *AISI 1045 Carbon Steel (UNS G10450)*. 2013 June 30, 2022]; Available from: https://www.azom.com/article.aspx?ArticleID=9153.

59. FYH, *Mounted Bearing Units*. Nippon Pillow Block Co., LDT.

60. *Bearing Units*. 2018, NTN Co.

61. F. P. BEER, E.R.J.J., J. T. DEWOLF, *Mechanics of Materials*. Vol. 5. 2009: Mc Graw Hill

62. Anderson, K., J.G. Kaufman, and J. Weritz, *ASM Handbook: Volume 2B Properties and Selection of Aluminum Alloys*. 2019: ASM International Materials Park, OH, USA.

63. *Custom Aluminum Framing Systems*, Inc., Editor.

64. *ASTM A36 Mild/Low Carbon Steel*. 2012 Jule 36, 2022]; Available from: https://www.azom.com/article.aspx?ArticleID=6117.